AMINE INHIBITION OF SILVER IODIDE ICE NUCLEATION

FINAL REPORT
NSF Grant ESR72-03349

Precipitation Process Modification Through Ice Nucleus Deactivation

Wm. Richard Barchet
Charles E. Anderson

Department of Meteorology
University of Wisconsin
1225 West Dayton Street
Madison, Wisconsin

December 1974

Amine Inhibition of Silver Iodide Ice Nucleation

Final Report

on

NSF Grant ESR72-03349 AO2
(Formerly Grant GI-31058)

"A Study of Precipitation Process Modification Through Ice Nucleus Deactivation".

by

Wm. Richard Barchet

Department of Meteorology
University of Wisconsin
Madison, Wisconsin

December 1974

Abstract

A quantitative evaluation was made of the degree to which a large number of amine compounds deactivate the ice nucleation ability of a silver iodide aerosol. Amine and other test substance concentrations could be produced over a wide range by a dynamic dilution system. Deactivation was quantified by comparing the ice crystal production of untreated and of treated silver iodide aerosols. These aerosols were generated by a hot-wire technique that made use of an improved method to coat the filament. Ice crystal counts were made in a small isothermal cloud settling chamber using a sugar solution as the crystal detector. Two amines demonstrated inhibition ability at 1 ppm while nine others showed an effect at higher concentrations. Two silanes gave inconclusive results.

Table of Contents

I. Introduction

This report serves to transmit a detailed description of the research activities and results obtain on NSF-RANN Grant GI-31058 "Precipitation process modification through ice nucleus inhibition" to the National Science Foundation.

Development of the various subsystems needed to evaluate the effects of trace gases on ice nucleation by silver iodide aerosols will be presented in approximate chronological sequence although much parallel development took place.

Research results concerning the action of eleven amine compounds and two silanes as ice nucleus inhibitors are presented in separate chapters.

1.1 Historical perspective

Much of the research on ice nuclei and ice nucleation processes received its initial impetus from the pioneering work by Vonnegut and by Schaefer at the General Electric Research Laboratory. Shortly after demonstrating the ability to artificially nucleate ice in clouds, Vonnegut (1948) and Schaefer (1949) reported that a wide variety of organic substances induced alterations of ice crystal habit. In a study on the deactivation of silver iodide ice nucleation ability by sunlight Reynolds, Hume and McWhirter (1952) discovered that ammonia appears to rejuvenate some of the deactivated aerosol.

These studies set the stage for the investigation by Birstein (1957) into the effect of adsorbed impurities on ice nucleation by lead and silver iodide aerosols. Birstein examined a wide range of substances and identified the organic amines as effective ice nucleation suppressants. His follow-up work (Birstein, 1960) highlighted the deactivation produced by methylamine and ethylamine. Shortly after Birstein's first report Poppoff and Sharp (1959) also examined the suppression of the ice nucleating ability of silver iodide by several substances. Their results were in substantial agreement with Birstein except for one point. Birstein has proposed a chemisorption mechanism for inhibition that was to be irreversible. Poppoff and Sharp however found the activity of the aerosol could be restored, if the sorbed material was caused to be desorbed; inhibition thus appeared to be a phenomena linked to physical adsorption. Table 1.1 presents a list of the various substances previously tested for their ability to inhibit ice nucleation. A very qualitative interpretation of each author's assessment of effectiveness is also given. Initials refer to the references cited.

Between 1960 and 1973 no experimental work on intentional ice nucleus inhibition was found by this author in the literature. Georgii (1963) did consider the potential of common air pollutants as ice nucleus inhibitors and found that ammonia and sulfur dioxide were of no consequence at the concentrations found in even heavily polluted air. It would appear that in these years the cloud physics community was preoccupied with techniques for increasing not decreasing the ice nucleus population of the atmosphere. Improved estimates of natural ice nucleus concentrations demonstrated that the optimum ice crystal concentration for precipitation development as found by Twomey (1958) and Juisto (1971) were often exceeded. Precipitation management needed a complement to ice nucleus seeding to handle such situations.

The concept that inhibition of ice nucleation by certain substances could function as a tool in precipitation process modification was revived nearly simultaneously by several investigators. In 1970, C. E. Anderson and W. R. Barchet of the University of Wisconsin proposed to examine ice nucleus suppression in the context of a hail mitigation tool. The research reported herein is a direct offshoot of that initial proposal. Elsewhere, P. St-Amand and W. Finnegan at the Naval Weapons Center, China Lake, California, also took an interest in ice nucleus inhibition by amines. And just recently work on the effect of isopropylamine on silver iodide ice nucleation was reported from Colorado State University, Fort Collins,

Colorado. One facet of the work at the Naval Weapons Center is represented in a report by Henderson and Duckering (1973) on the response of small cumulus clouds to treatment with morpholine or with ethylamine. Based on observations of cloud evolution morpholine appeared to inhibit glaciation and stimulate rain, while ethylamine had no apparent effect on precipitation but may have stimulated glaciation. At Colorado State University, Haines (1974) reported in a masters thesis that although isopropylamine largely inhibits nucleation, in a narrow range of concentrations this substance enhances the ice nucleation activity of a silver iodide aerosol derived from a $AgI-NH_4I$ acetone solution burning generator.

To place this report and the studies mentioned above in their proper historical perspective we can say that 15 years ago the door was opened and we are just now beginning to take the steps that may eventually lead to the development of ice nucleus inhibition as a viable precipitation modification technology. This report is another step in that direction.

Table 1.1 A summary of ice nucleation inhibition by substances previously tested.

Substance	Inhibition Effect	Reference
Ethylamine	Very good	B
Methylamine	Very good	B
Sec-Butylamine	Good	B,P-S
Dimethylamine	Good	B
Isopropylamine	Good	P-S,H
Trimethylamine	Fair	B
Ammonia	Fair-Poor	B,P-S,G
Butylalcohol	Poor	P-S
Ethanol	Poor	B,P-S
Isopropanol	Poor	P-S
Methanol	Poor	P-S
Sulfur dioxide	Very poor	G
Bromobenzene	None	B
Diethylether	None	B
Ethylene glycol	None	B
Isobutane	None	B
n-Heptane	None	B
Propylene glycol	None	B

1.2 Preface to developmental work

Three subsystems are crucial to the investigation of ice nucleation inhibition by trace vapors. At the University of Wisconsin, each of these subsystems had to be developed and constructed from, so to say, the ground up. Much of the grant period was concerned with the development of these subsystems.

In order to provide a wide range of trace vapor concentration and to permit exposure of the ice nucleus aerosol to the trace vapor at normal temperatures, we developed a dynamic trace vapor dilution system. Pure vapors or saturated carriers could be input to the system and the output concentration varied from one part per thousand to less than one part per trillion by a series of dilution stages. The dynamic nature of the dilution system made compensations for wall losses unnecessary and assured concentration uniformity throughout the system.

Our test aerosol, silver iodide, was chosen for its wide spread use and rather well characterized behavior as an ice nucleant. Generation of the aerosol required a technique free of potential side products which could interfere with the test substance. We developed a new approach to the generation of a silver iodide aerosol using a plated hot wire aerosol source. Such plated wires were found to provide adequate output and to demonstrate good temporal stability.

The final and perhaps the most crucial component of our experiment is our ice nucleus counting system. Following the recommendations of a recent ice nucleus counter intercomparison workshop, we designed and built an isothermal cloud settling chamber. A moist, heated top plate provided via diffusion water vapor for condensation into droplets which settled throughout the depth of chamber. Ice crystals grown on ice nuclei activated within the isothermal portion of the chamber fell into a supercooled sugar solution, where they could grow to a countable size. This device was admirably suited for ice nucleus counts with our silver iodide aerosol and with minor modifications

could be used to study natural nuclei.

A view of the entire system as it appeared in operation is seen in Fig.1.1 Each major subassembly is visible. The components parts of most of the subassemblies are described in detail in the text.

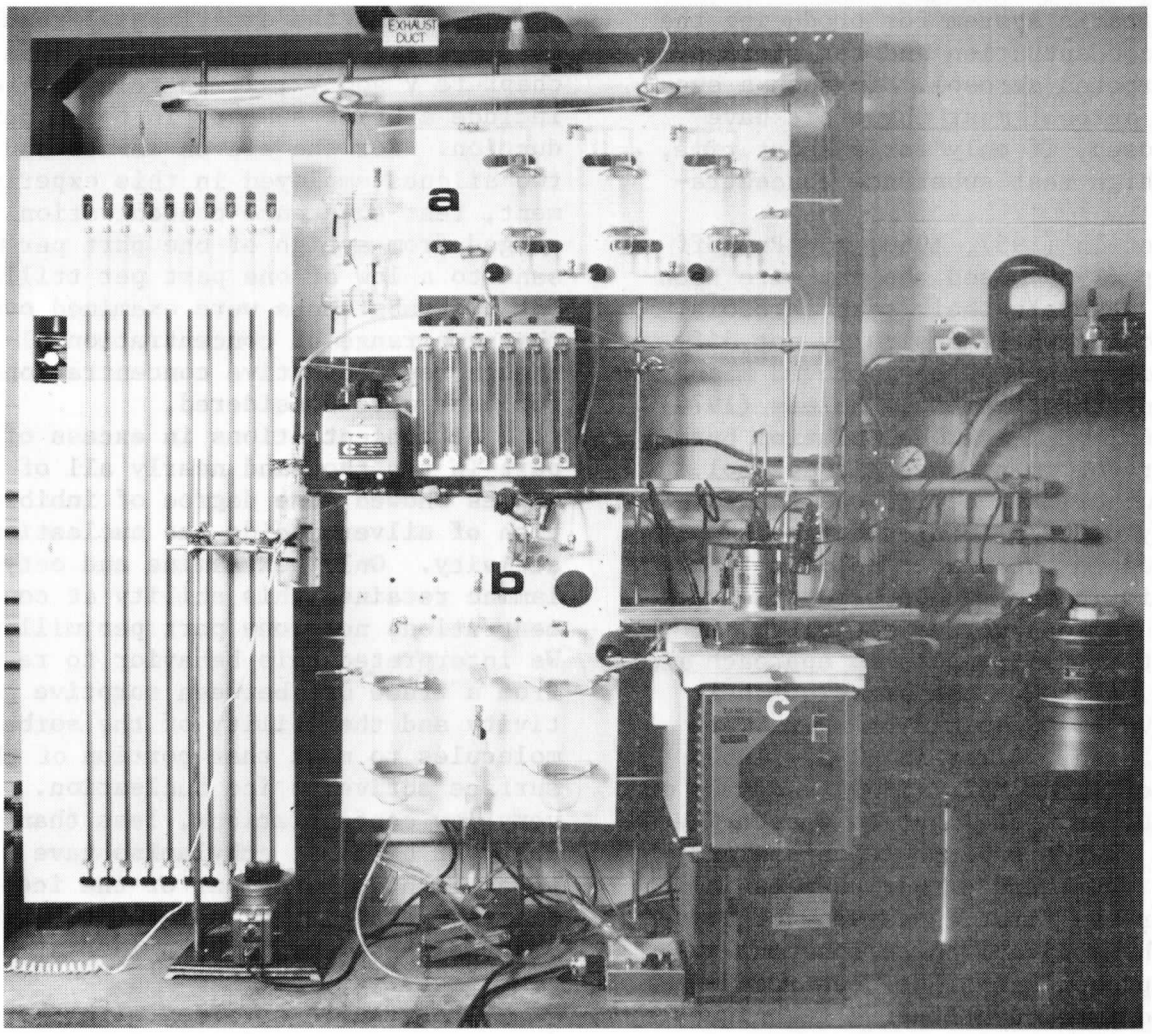

Figure 1.1. Full view of ice nucleation inhibition test system: (a) Dilution system components, (b) AgI aerosol generator components, (c) Cloud chamber components.

1.3 Comparison to previous experimental techniques

In all previous investigations of ice nucleus inhibitors, the same basic subsystem are found. However, the approaches taken to provide the function of those subsystems were often different.

Test substances concentration can be produced by a dynamic or a static approach. We have used the dynamic approach with multiple dilution stages. Birstein (1957) controlled the concentration of test substance by maintaining a sample of the test liquid at constant temperature and passing the aerosol laden air over the cold liquid. Adsorption of the vapor, therefore, took place in an environment saturated with the vapor and at temperatures much below those normally encountered in clouds. Poppoff and Sharp (1959), on the other hand, permitted, as we have, the aerosol and vapor to interact at

more representative temperatures by mixing a vapor-laden air stream with an aerosol-laden flow. Birstein (1960), by changing from a dynamic system to a static one, was able to avoid the difficulty of low temperature exposure of his aerosol but still retained cryogenic control over test substance concentration. Haines (1974) made use of a completely static system for producing the desired concentration and for storage of the exposed aerosol. In such a system some aerosol must therefore have been exposed, if only for a short time, to very high test substance concentrations.

Birstein (1957, 1960) and Poppoff and Sharp (1959) used the hot-wire technique to generate their test aerosols. Our approach, while basically not different, does involve an improved means of coating the filament. Haines (1974) used an AgI-NH_4I acetone solution burning generator to produce his aerosol. The output of this device was then dynamically diluted to provide the sample introduced to the static holding tank.

It is in the method used to detect and measure ice nucleus activity that the greatest differences in approach are evident. Although the sizes of their respective mixing cloud chambers were much different, Birstein (1957, 1960) and Poppoff and Sharp (1959) made use of a parallel beam of light to detect ice crystals in the supercooled cloud and visually estimated either changes in number or the first appearance of crystals. The subjectiveness inherent in their approach has since been recognized and more quantitative techniques have been developed to avoid this situation. Haines (1974) determined crystal concentrations in the large Colorado State University isothermal cloud chamber by counting the crystals which fell onto microscope slides on the bottom of the chamber. The use of a supercooled sugar solution as in our isothermal cloud settling chamber is a well known method of obtaining an integrated count of activated ice nuclei.

Our approach to ice nucleus inhibition differs from all the others in that it involves the comparison of the number of ice crystals produced by a test or treated aerosol to the number of crystals derived from a clean aerosol. We are therefore able to assess quantitatively the degree of inhibition and the statistical confidence that can be placed on that assessment.

1.4 Summary of results.

Although the experimental results obtained are discussed in detail in chapters V and VI, it is relevant to include a brief summary in this introduction. For the eleven amines and two silanes employed in this experiment, test substance concentration ranged from a high of one part per thousand to a low of one part per trillion. Not all substances were examined over the same range of concentration although representative concentrations for each were considered.

At concentrations in excess of one part in ten thousand nearly all of the amines showed some degree of inhibition of silver iodide ice nucleation activity. Only hexylamine and octylamine retained this ability at concentrations near one part per million. We interpreted this behavior to result from a trade off between sorptive activity and the ability of the sorbed molecules to mask that portion of the surface active in ice nucleation. At very low concentrations, less than one part per billion, ethylamine gave rise to a slight enhancement of the ice nucleation activity of our aerosol; the other amines were not examined at such low concentrations.

The results obtained with the silanes were not nearly as clear cut as with the amines. At low concentrations inhibition of ice nucleation was observed while at high concentrations an apparent enhancement was produced. We can only offer a tentative explanation based on the reactivity of the silanes with water. At high concentrations, sorption of large amounts of silane assists the condensation activity of the aerosol thereby promoting freezing nucleation. At lower concentration, sorption primarily affects the ice nucleation active surface sites and thus inhibits nucleation.

Table 1.2 summarizes the inhibition activity of the substances dealt with in this study in much the same fashion as Table 1.1 considered previously tested materials. The behavior of these compounds at essentially the same concentration was used to give a qualitative estimate of their relative effectiveness as ice nucleation inhibitors. Quantitative data is available in Chapters V and VI.

Table 1.2 A summary of ice nucleation inhibition by amines and silanes tested in this study.

Compound	Inhibition Effect
Hexylamine	Very Good
Octylamine	Very Good
Pyridine	Good
Ethylamine	Good
Butylamine	Good
2.4 Lutidine	Fair
Morpholine	Fair
Dimethylamine	Poor
Methylamine	Poor
Dodecylamine	None
Benzylamine	None
Dichloro dimethyl silane	Good
Diethoxy dimethy silane	Fair

II. Trace Vapor Dynamic Dilution System

The first of the three major subsystems to be described is the dynamic dilution system. Each of the components of this system is described in detail. A mathematical model of the operation of the dilution apparatus is presented along with an error analysis that permits confidence intervals to be placed on the output test gas concentration.

2.1 Clean air supply

The voluminous flows of clean air required to operate a dynamic dilution system could not be economically provided by bottled, purified air. Instead we adapted the method of Feeley and Kunnas (1961) to dry and purify our in-house compressed air supply. A photograph of the air drying apparatus is given in Fig. 2.1.

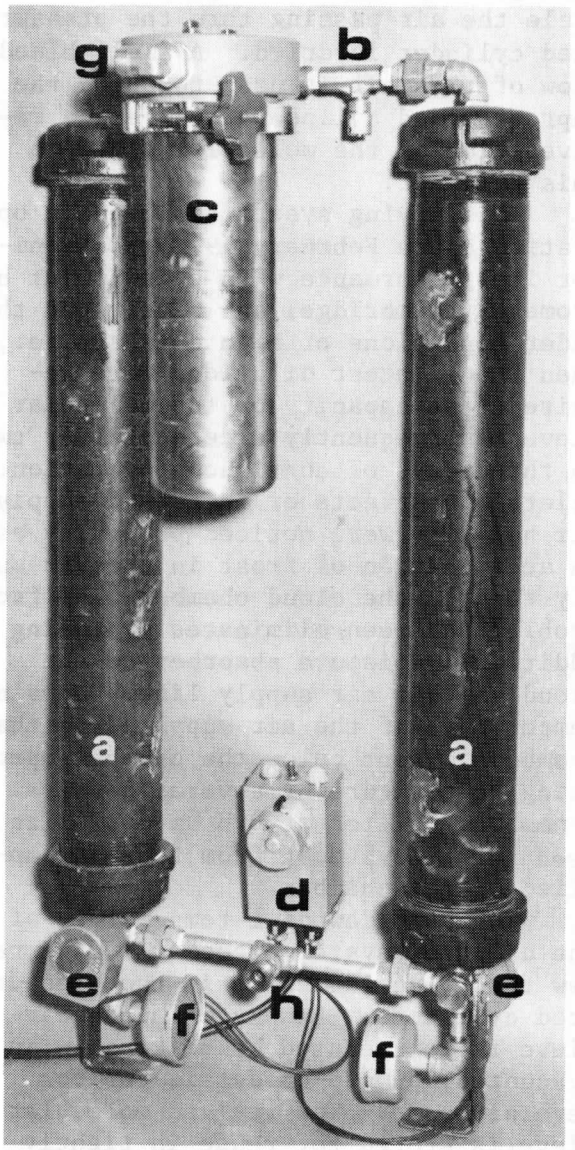

Figure 2.1. Air drying and purifying apparatus: (a) adsorbate cylinders, (b) metering-check valve, (c) membrane prefilter, (d) timing device, (e) 3-way solenoid valves, (f) mufflers, (g)clean air output, (h) house compressed air input.

Molecular sieve sorbents, types 13X and 5A are contained in steel cylinders. Under high pressure, 80 lb/in^2, molecular sieve absorbs water vapor. At low pressure, ambient atmospheric, the excess water sorbed by the molecular sieve is given off to a dry air purge. A timing device and appropriate solenoid, check, and needled valves alter-

nately pressurize and vent the cylinders. During the pressurized portion of the cycle the air passing thru the pressurized cylinder is dried. A small bleed flow of this air is used to purge the unpressurized cylinder to affect a rejuvenation of the molecular sieve in this cylinder.

This drying system has been in operation since February 1972. We monitor its performance with a dew point hygrometer (Cambridge) and have found that under conditions of high demand, i.e., when the greatest dilutions were required, the capacity of the molecular sieve was frequently exceeded after two to three days of continuous operation. Deletrious effects of increased supply air humidity were noticed primarily as an accumulation of frost in the air supply tube to the cloud chamber. The frost problem has been eliminated by adding an additional moisture absorber to the cloud chamber air supply line. Dewpoint temperature of the air supplied to the chamber is kept below the chamber operating temperature by several degrees. A membrane filter of 0.8 μm pore size is used to remove dust from the air supplied to the chamber.

When the dewpoint temperature of the dilution system exceeds -10C we renew the molecular sieve in the pressurized cylinders. Exhausted molecular sieve is rejuvenated by heating in an evacuated, pumped-on dessicator for several hours. The revived molecular sieve is stored for reuse in tightly capped bottles. Similar procedures are used to rejuvenate the calcium sulphate in the final drying column in the cloud chamber air supply line.

Particulate matter is removed from the supply air before entering the distribution system by a membrane pre-filter (Millipore MF Lifegard II) element with nominal 0.3μm pore size. This filter is changed at six month intervals; no problem with excessive blockage of filter has been thus far encountered.

2.2 Distribution System

A pressure regulator (Matheson 402) reduces the high pressure clean air supply to 20 psig. This air is distributed to various system components through a distribution manifold (Tap Tube 1830-2) with twelve quick connect-disconnect fittings. During system operation at different flow rates the pressure regulator is always adjusted to maintain 20 psig pressure in the distribution manifold to insure reproducible flow rates in the various system components.

A large number of system elements are served by a flowmeter panel holding a series of rotameter flow gages and multiturn needle flow control valves (Brooks Sho-Rate 1355-8506). Several ranges of flow rates are available and additional flexibility is possible with the use of different floats in the meters. The length of the vinyl tubing (Mayon R220) to the flowmeter panel and from the flowmeter panel to the dilution system was kept the same for all flowmeters so that the meters could be reliably interchanged.

Some of the trace vapors used in the dilution system exhibited reactions with even trace quantities of moisture. The flowmeters used with the dilution system were also provided with an optional dry nitrogen supply at 20 psig. This provision was used only with the water reactive trace vapors.

2.3 Flowmeter calibration

Each flowmeter and its associated dilution vessel, when possible, was calibrated to cover a wide range of flow rates and system pressures. The volume flow rate was determined with the use of a wet test gas flowmeter (Precision Scientific) on loan from the Department of Chemical Engineering. The elapsed time for the displacement of a minimum of 0.1 cubic foot (2832 cm^3) was measured with an electronic digital timer (Anaconic 390). At high flowrates displacements as large as 1.0 cubic foot were used.

The volume rate of flow ($\dot{V}$) for each setting of the rotameter flow was determined with the aid of the flowing equation

$$\dot{V} = \frac{P+p_m}{P+p} \frac{T_r}{T_m} \frac{1+w}{1+w_m} \frac{\Delta V_m}{\Delta t} \qquad 2.2.1$$

where the over-dot represents a differ-

ential with respect to time, i.e., a rate. The central parameters are the displacement indicated by the wet test meter (ΔV_m) and elapsed time (Δt); the other parameters are dependent on the experimental conditions. The ambient air pressure (P) is increased by the pressure drop across the meter (p_m) which affects the volume measured and the internal over pressure (p) within the dilution system itself. Temperature correction must also be applied since the ambient air temperature (T_r) is usually higher than the temperature (T_m) within the wet test meter. Evaporation of the meter fluid, water, causes an increase in the molar mixing ratio (w) of the air passing through the meter to saturation and alters the apparent volume flow.

The three calibration curves given in Fig. 2.2 have been extrapolated to p = 0 and must be corrected by a small amount for the elevation over ambient of pressure (p) within the dilution vessel as measured on a manometer to be described later. The correction expressions for volume flow in liters per minute with p(cm) are:

$$\text{Flowmeter A: } \dot{V} = \dot{V}_o - 0.0043\ p$$

$$\text{Flowmeter B: } \dot{V} = \dot{V}_o - 0.0025\ p \quad 2.2.2$$

$$\text{Flowmeter C: } \dot{V} = \dot{V}_o - 0.0022\ p$$

Three additional rotameter type flowmeters were also calibrated using the same procedure but due to the much smaller flow rates no system pressure dependence was observed. The calibration curves for these flowmeters are given in Fig. 2.3.

It is estimated that the flows determined from the calibration curves are accurate to better than 5%. This value will be used in subsequent discussions of error estimates.

2.4 Manometer panel

Pressure differences and system pressures are very important in the operation of a dynamic dilution system. Ten manometers connected to a common reference arm are mounted on a single panel. Each manometer has a fluid trap to prevent manometer fluid from enter-

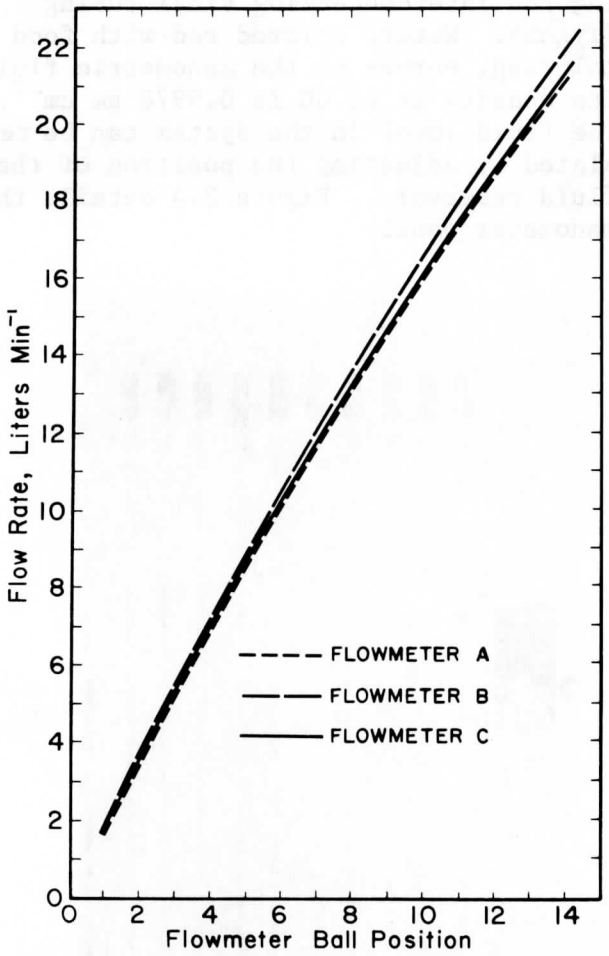

Figure 2.2. Zero back-pressure flowmeter calibration curves for large Rotometers.

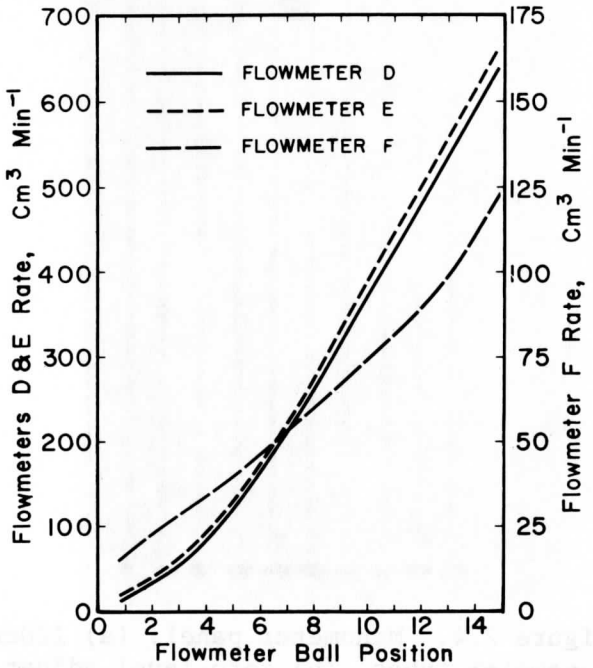

Figure 2.3. Calibration curves for small Rotometers.

ing the interconnecting vinyl tubing (Tygon). Water, colored red with food coloring, serves as the manometric fluid. Its density at 23.6C is 0.9978 gm cm^{-3}. The fluid level in the system can be regulated by adjusting the position of the fluid reservoir. Figure 2.4 details the manometer panel.

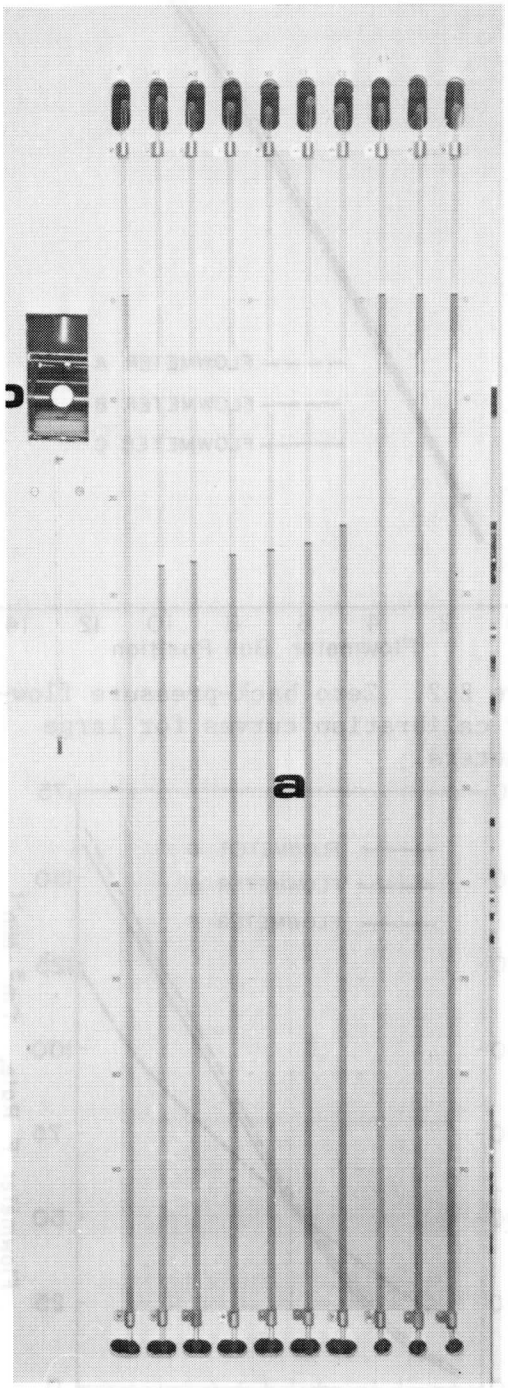

Figure 2.4. Manometer panel: (a) 120cm manometer tubes, (b) zero level adjust with fluid reservoir.

2.5 Dilution vessel

The central element to a dynamic dilution system is the mixing vessel in which the air stream to be diluted is mixed with a diluent, pure air flow. Figure 2.5 details the pyrex glass dilution vessel panel. The input flow to each vessel enters at A while the diluent enters at B. An extended probe (C) samples the air on the axis of the vessel and away from the exhaust port D. Side arms E and F are used to connect the dilution chamber to a manometer panel for pressure measurement. Capillary flow tube G interconnects two dilution vessels.

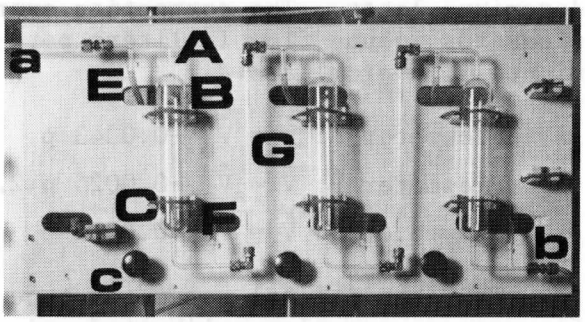

Figure 2.5. Three dilution vessels mounted on single panel with capillary flow tubes in place. Input to dilution system at (a), output from last dilution vessel at (b). Valves (c) are used to adjust back pressure in each vessel and lead to exhaust duct.

2.6 Concentration computation and error analysis

The dilution achieved in each dilution chamber depends on the ratio of input flow and total flow rate within the vessel. The output concentration (C_{out}) for any dilution stage is given by

$$C_{out} = \frac{\dot{V}_i}{\dot{V}_i+\dot{V}_d} C_{in} \qquad 2.6.1$$

where C_{in} is the input concentration and $\dot{V}_i$ and $\dot{V}_d$ are the input and diluent flow rates, respectively. This expression can be reduced to

$$C_{out} = \frac{1}{1+R-C_{in}} \; C_{in} \qquad 2.6.2$$

where $R = \dot{V}_d/\dot{V}_i$, the ratio of diluent to input flow rates.

When a series of N dilution stages are used the final output concentration is given by a product of the dilutions produced at each stage:

$$C_{out} = C_{in}^{\circ} \prod_{k=1}^{N} (1 + R_k)^{-1} \qquad 2.6.3$$

where C_{in}° is the initial concentration of trace vapor in the input flow to the first dilution vessel and R_k is the flow ratio for the k^{th} dilution chamber.

An error estimate based on an analysis of the variance of the dilution gives a fractional variance of the output concentration of any stage as

$$\frac{\sigma^2(C_{out})}{C_{out}^2} = \left[\frac{1+R}{1+R-C_{in}}\right]^2 \frac{\sigma^2(C_{in})}{C_{in}^2} + \left[\frac{R}{1+R-C_{in}}\right]^2 \frac{\sigma^2(R)}{R^2} \; . \qquad 2.6.4$$

The fractional variance of the dilution ratio R is given by the accuracy to which each flow can be determined

$$\frac{\sigma^2(R)}{R^2} = \frac{\sigma^2(\dot{V}_i)}{\dot{V}_i^2} + \frac{\sigma^2(\dot{V}_d)}{\dot{V}_d^2} \; . \qquad 2.6.5$$

The result of this analysis indicates that the most reliable estimate of output concentration is obtained when the dilution at each stage is as large as possible and the number of dilution stages kept to a minimum. In practice the minimum is usually two and for very small concentrations may be as large as five.

2.7 Calibration of dilution chamber input flows

The transfer of trace gas from one dilution chamber to another occurs through a fine interconnecting capillary tube. A 2 cm length of 1 mm bore pyrex capillary tubing is fused to two lengths of 6 mm O.D. pyrex tubing which mate with the fittings used to insert capillary into system. The fine capillary is drawn by heating the section of 1 mm capillary tubing and stretching to approximately 10 cm length.

Pipe flow theory (Lamb, 1932) indicates the volume flow out of a capillary is proportional to the pressure drop (Δp) across the capillary and is dependent on the mean pressure ($\bar{P}$) within the capillary and the pressure P_i at the exit end of the capillary:

$$\dot{V}_i = K \frac{\bar{P}}{P_i} \; \Delta p. \qquad 2.7.1$$

The pressures $\bar{P}$ and P_i are related through Δp

$$\bar{P} = P_i + \Delta p/2 \qquad 2.7.2$$

and the magnitude of Δp is so small in comparison to P_i, which depends primarily on the ambient air pressure, that the flow equation effectively reduces to

$$\dot{V}_i = K\Delta p \qquad 2.7.3$$

Very small flow rates were measured with a soap bubble flow meter. A stop watch was used to measure the elapsed time (Δt) for a given volume displacement (ΔV). The quantity $\dot{V}_i$ was computed from $\Delta V/\Delta t$ and normalized to standard temperature and pressure. A least square regression analysis forced through the origin was used to evaluate the proportionality constant K. Table 2.1 gives the slope found for each capillary tube in which Δp has units of centimeters of water. The error terms apply to the value of the proportionality constant.

The standard deviation of the slope allows the fractional variance of the input flow to each dilution vessel to be determined:

$$\frac{\sigma^2(\dot{V}_i)}{V_i^2} = \frac{\sigma^2(K)}{K^2} + \frac{\sigma^2(\Delta p)}{(\Delta p)^2} \qquad 2.7.4$$

In practice Δp can be determined to ±1mm and if we assume this to be the error estimate for all measurements

$$\sigma^2(\Delta p) = 0.01 \text{ cm}^2. \qquad 2.7.5$$

Table 2.1 Capillary flow tube rate constants.

Capillary Tube	K $cm^3 min^{-1} cm^{-1}$	$\sigma(K)$	$\sigma^2(K)/K^2$
A	0.6473	.09	.019
B	0.5098	.10	.038
C	0.3827	.14	.134
D	0.3641	.14	.148
E	0.4905	.12	.060
F	0.3680	.04	.012

2.8 Trace vapor sources

The compound which is to be introduced into the air stream and subsequently diluted may have a vapor pressure above or below ambient atmospheric pressure at the temperature of the laboratory. Those compounds with a vapor pressure above ambient can be introduced to the system as a pure vapor usually supplied in lecture bottles. The concentration of this vapor is taken to be unity.

If, however, the vapor pressure of the compound is below ambient the material exists as a stable, though volatile liquid which introduces additional problems in getting the material into the air stream. Our approach is to saturate a stream of air or nitrogen bubbled through the liquid. A series of two bubblers (Ace Glass 7532) is used with the first heated and the second immersed in an ice bath. In the heated bubbler the vapor is supersaturated with respect to the second colder bubbler in which excess vapor is removed. The saturation vapor pressure p_s of the liquid at the ice point is used to calculate the concentration of trace vapor in the air leaving the second bubbler:

$$C^\circ_{in} = \frac{p_s}{P} \text{ and } \frac{\sigma^2 C^\circ_{in}}{C^{\circ\,2}_{in}} = \frac{\sigma^2 p_s}{p_s^2} + \frac{\sigma^2 P}{P^2} \qquad 2.8.1$$

where P is the total pressure at the exit of the bubbler. The entire air flow through the bubbler becomes the input flow to either the first dilution vessel, or to the Wösthoff gas dosing device.

Since p_s is determined by the temperature of the final bubbler an estimate of the error associated with the value of p_s can be derived from the integrated form of the Clausius-Clapeyrom expression for saturation vapor pressure:

$$p_s = A\, e^{B/T} \qquad 2.8.2$$

where A and B are constants and T is the Kelvin temperature. From this expression we find:

$$\frac{\sigma^2_{p_s}}{p_s^2} = \frac{B^2}{T^4}\sigma_T^2 \qquad 2.8.3$$

where σ_T is the standard deviation of the temperature in final bubbler.

2.9 Wösthoff gas dosing device

The introduction of pure trace substance vapor directly into the dilution system has one basic drawback, the rate of flow of the vapor is very difficult to determine yet critical to the dilution computation. To overcome this and other problems associated with high concentrations of trace material in the manometer system we included a Wösthoff gas dosing device, model 1DS/2, as the initial dilution stage.

The dosing device consists of a rotating stopcock with a precisely known bore volume. As the stopcock rotates 180° from one rest position to another it is alternately filled with the air stream to be diluted and purged by the diluent flow. In our application the stream to be diluted may be the pure trace compound vapor as supplied from a lecture bottle or the out-

put of a bubbler train as described above.

When in operation the output of the dosing device will undergo step-function changes in trace gas concentration due to cyclic, pulse-wise additions of trace vapor to the diluent carrier air stream. To make the output more uniform, a series of mixing vessels is placed downstream from the dosing device. A differential equation describing the effect of a mixing vessel on the concentration was presented by Axelrod, et al.,(1970):

$$\dot{C}_k = (C_{k-1} - C_k)\frac{F}{V_k} \qquad 2.9.1$$

where C_k and C_{k-1} are the concentration of trace vapor in the flow out of and into the k^{th} mixing vessel of volume V_k, respectively, and F is the volume rate of flow through the mixing vessel. This equation was solved for a series of mixing vessels on the Applied Dynamics-32 analog computer in the Department of Electrical and Computer Engineering. The diagram of Fig. 2.6a gives the analog circuit used to simulate a series of three mixing vessels.

The output of the dosing device and input to the first mixing vessel was simulated by a rectangular pulse of amplitude C_o = 0.625 which takes into account a realistic proportioning of the diluent flow (F) between the stopcock bore and a continuous by-pass. The pulse repetition rate was specified by the interval between stopcock rotations (6 to 60 seconds). The duration (τ) of the pulse from the dosing device is dependent on the volume of the stopcock bore (V_o) and flow rate of diluent stream through the stopcock (0.6 F):

$$\tau = \frac{V_o}{0.6\ F} \qquad 2.9.2$$

The steady state, average concentration of the dosing device output flow is given by

$$C_\infty = \frac{V_o \nu}{F} \qquad 2.9.3$$

where ν is the frequency (1 to 10 min^{-1}) at which the stopcock cycles. This frequently is regulated by synchronization with the standard 60 Hz AC frequency. We currently have a Viton A stopcock

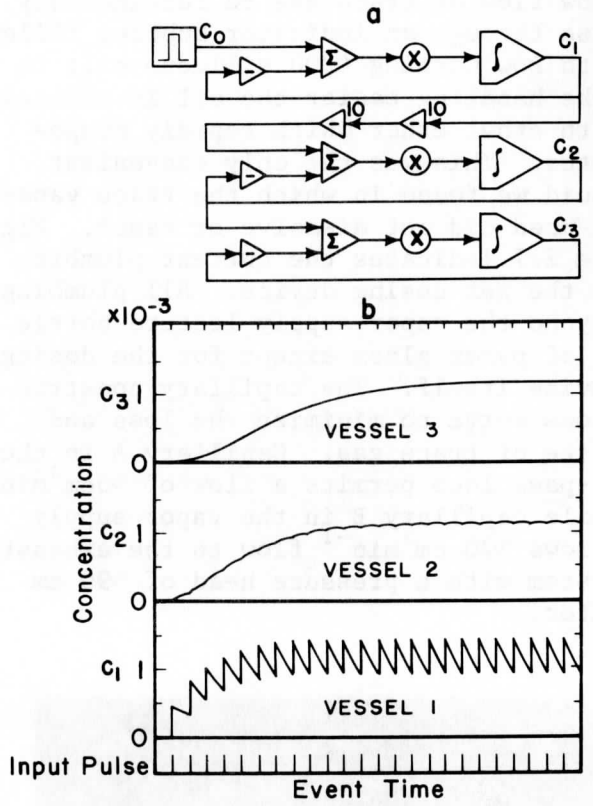

Figure 2.6. Results of an analog simulation of the output from a Wösthoff gas dosing device. Analog circuit shown in (a) while results of simulation for three 100 cm^3 mixing vessels, a flowrate of 400 $cm^3 min^{-1}$ and a final concentration of 1.2 x 10^{-3} are shown in (b). Input pulse width 23 m sec with pulse repetition rate of 5 min^{-1}.

with V_o = 0.0493 cm^3 and a Teflon stopcock with V_o = 0.0930 cm^3. According to the manufacture these volumes are accurate to 0.0002 cm^3.

Figure 2.6b shows the results of one analog computer experiment in which V = 100 cm^3, F = 400 $cm^3 min^{-1}$, and C_∞ = 1.2 x 10^{-3}. From this figure it is clear that three mixing vessels reduce the oscillations in the output concentration to an insignificant level. The smoothing effect is increased if V or ν increases or F decreases. Based on these results we are using a series of three 100 cm^3 mixing vessels and a diluent flow rate of 500 $cm^3 min^{-1}$.

Several plumbing modifications were made on the original gas dosing unit. These modifications allow a very

slow flow of trace gas to continuously pass through an indicator bubbler filled with Dow Corning #200 silicone oil; to make handling easier the oil is thinned with ethyl ether which rapidly evaporates. This was the only convenient fluid we found in which the trace vapors we used did not dissolve or react. Figure 2.7 indicates the current plumbing on the gas dosing device. All plumbing beyond the vapor supply lecture bottle is of pyrex glass except for the dosing device itself. The capillary constrictions serve to minimize the loss and waste of trace gas. Capillary A in the by-pass loop permits a flow of $\sim 5 cm^3 min^{-1}$ while capillary B in the vapor supply allows $\sim 20\ cm^3 min^{-1}$ flow to the exhaust system with a pressure head of ~ 90 cm water.

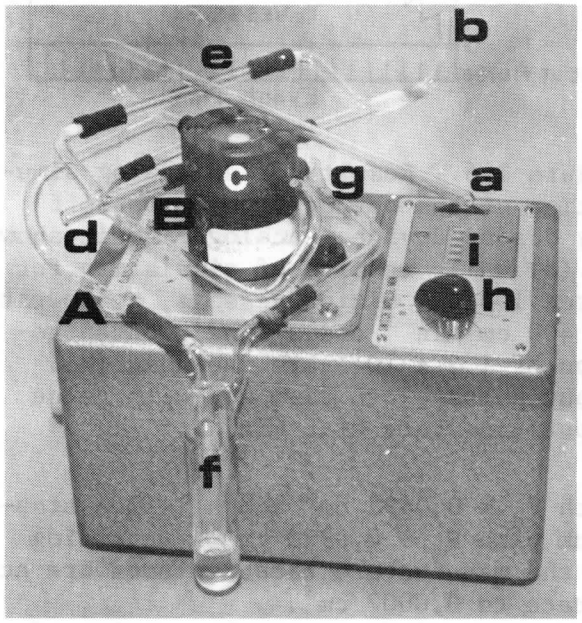

Figure 2.7. Plumbing modifications on Wösthoff gas dosing device: (a) vapor source input, (b) diluent input, (c) rotating stopcock, (d) dosing device output, (e) diluent by-pass, (f) vapor source flow indicator, (g) waste gas exhaust, (h) pulse repetition rate selector, (i) pulse counter.

The dosing device originally purchased was equipped with a Viton A stopcock plug. However after only a short period of operation the bore became fouled with residue produced by a reaction between the amine compound used as a trace gas and stopcock material. Inquiry to the distributor prior to ordering had given no indication of this problem. After the problem was brought to the attention of the distributor a teflon plug was provided at no additional charge. This plug is still in use and upon examination after several months operation showed no deterioration.

The entire stopcock housing is vented to the laboratory hood exhaust system because the teflon plug is not meant to seal gas-tight in the stopcock body. Permeation losses through the teflon plug also occur but pose no problem in our application.

An error estimate for the average concentration of trace gas in the carrier stream leaving the gas dosing device is given by:

$$\frac{\sigma^2(C_\infty)}{C_\infty^2} = \frac{\sigma^2(V_o)}{V_o^2} + \frac{\sigma^2(\nu)}{\nu^2} + \frac{\sigma^2(F)}{F^2} \qquad 2.9.4$$

According to the manufacture $\sigma^2(\nu) \doteq 0$ while the V_o term is 5×10^{-5} and 17×10^{-5} for the Teflon and Viton A stopcocks, respectively. This leaves the carrier gas flow rate as the major contributor to uncertainty in the output concentration. Flowmeter E is generally used to provide the carrier flow for the dosing device and the entire flow enters the first dilution chamber.

2.10 Calibration of dilution system

In our original proposal we had planned to check the operation of the dilution system by a direct chemical analysis of the effluent for the trace gas concentration. However during the course of our research no suitable means for direct chemical analysis was found. Such analysis could have been useful to examine the response of our dynamic dilution system to changes in vapor concentration. However most analysis techniques, Hong and Connors (1968) for instance, require such a long sampling time at the concentra-

tions of interest that the transient behavior of amine concentration would be obscured.

We have, therefore, based our estimates of test gas concentration on our dilution computations and error analysis. In order to avoid the possibility of concentration transients we allow a minimum of three hours for system equilibration after a concentration change. A twenty-four hour purge with clean air between tests with different test substances should prevent one substance from interfering with the results of another. In some instances portions of the interconnecting plumbing is also replaced to avoid interference.

III. The Cloud Chamber

3.1 Choice of design

The most recent inter-comparisons of cloud chambers and techniques for ice nuclei measurement are reported in the procedings of the Second International Workshop on Condensation and Ice Nuclei held in Fort Collins, Colorado in August 1970. In this report three ice nucleus counting devices received high ratings: (1) the cloud settling chamber of Ohtake, (2) the Goetz aerosol spectrometer, and (3) the membrane filter method of Gagin. Devices (2)and (3) require sophisticated apparatus and were considered too expensive for our application. The Ohtake technique offers the most direct and simplest approach to ice nuclei activation and counting.

In principle the cloud chamber is a combination of a thermal gradient diffusion chamber in which the cloud is formed and an isothermal cloud chamber in which the ice nuclei are activated. The cloud formed in the thermal gradient section settles into the subfreezing isothermal section and provides a realistic simulation of natural cloud conditions for ice nuclei. All mechanisms of ice nucleus activation can operate within the chamber.

3.2 Physical description

The cloud chamber proper shown in Figure 3.1 is a brass cylinder 14.5 cm inside diameter and 25 cm deep. This cylinder is immersed into a constant temperature bath (Neslab-Tamson TE10) to a depth of 20 cm. Retaining tabs allow the cylinder to be latched in place with 5 cm of the brass external to the bath. Following the design of Ohtake (1970) a plexiglass collar 7 cm high of same internal dimension as the chamber is fastened to the top of the chamber giving the chamber a total volume of 5.28 liters; a viton O-ring insures a tight seal. The top of the chamber is covered by a moveable plexiglass slide which can be positioned to allow access to chamber, to view chamber, or to place the vapor source above the chamber.

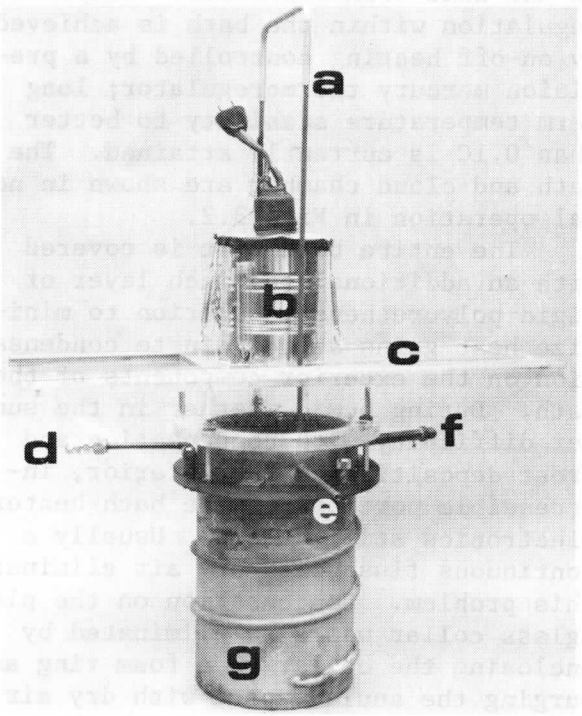

Figure 3.1. Assembled isothermal cloud setting chamber: (a) pushrods to manipulate glycerine roller, (b) cloud generator, (c) sliding plexiglass top, (d) purge air inlet, (e) sample injection port, (f) exhaust port, (g) brass cylinder.

A coil of 1/4" O.D. copper tubing soldered to the outside of the cylinder carries the purge air supply to an inlet 2 cm above the inside bottom of the chamber. Two other ports are located

at 22.5 cm above the bottom. One of these ports serves as the ice nucleus sample injection port. The other port currently functions as an exhaust port although in an earlier version of the chamber it was intended to be the moist air inlet.

3.3 Bath temperature control system

The Tamson bath is cooled by a Flexicool, model FC-20-40-P3-SV portable refrigerator unit. The cooling probe is a stainless steel coil 5 cm in diameter and 20 cm long with an effective surface area of 729 cm^2. Methyl alcohol is used as the working fluid in the bath; the lower 16 cm of the brass cloud chamber cylinder is immensed within the heat transfer fluid. Temperature regulation within the bath is achieved by on-off heating controlled by a precision mercury thermoregulator; long term temperature stability to better than 0.1C is currently attained. The bath and cloud chamber are shown in normal operation in Fig. 3.2.

The entire bath unit is covered with an additional one inch layer of rigid polyurethene insulation to minimize heat gains and eliminate condensation on the exterior components of the bath. During humid weather in the summer difficulty with condensation and frost deposition on the interior, inaccessible portions of the bath heater electronics still occurs. Usually a continuous flush with dry air eliminates this problem. Condensation on the plexiglass collar was also eliminated by enclosing the collar in a foam ring and purging the anular space with dry air.

We did have problems with the Flexicool unit. After only two months of duty we were unable to maintain working temperature of -16C. Supplemental cooling was obtained by circulating the heat transfer fluid through a dry ice heat exchange unit. With this operation rapid cool down was possible and the working temperature could be maintained. However it became necessary to use more and more dry ice to maintain the required heat pumping capacity.

A check with a local refrigeration repair shop disclosed a loss of working fluid Freon 13B1 and also that Freon 502 would provide a greater heat exchange rate although with a warmer absolute minimum attainable temperature. The manufacturer indicated the change in working fluid would cause no problems with unit so we replaced the original working fluid with Freon 502 in September 1973. No cooling difficiency has been noted since.

3.4 Cloud generation

The diffusion of water vapor downward from the top of the chamber into a region of decreasing temperature leads to a supersaturated environment and the formation of a cloud. Cloud droplets form on the available nuclei in the purge air. As they grow the droplets begin to settle out of the supersaturated region and into the drier portion of the chamber. Here they evaporate and increase the moisture content. Within a few minutes droplets are able to survive the fall to the bottom of the chamber and the entire chamber approaches water saturation. It is within this environment that the ice nuclei are activated.

Moisture is supplied to the chamber by evaporation from a moist pad of filter paper held at 38-44 C. A stainless steel screen supports the filter paper. Water is added to the pad through a capillary feed tube from a reservoir. Our original design made use of a hot plate to which a thin sponge had been glued. However the large thermal mass of the hot plate made temperature regulation very poor. In our present system the filter paper is in contact with the under surface of a thin metal plate. The upper surface of the plate is radiatively heated by a 100 watt incadescent lamp. Temperature sensing and control is obtained with a thermistor sensor in contact with the moist filter paper. The thermister is one arm of an AC resistance bridge. Bridge imbalance activates a zero crossing electronic switch to turn the lamp on and off. When at operating temperature the lamp flashes on and off at around 2 Hz. An expanded view of the cloud generator is shown in Fig. 3.3a with a circuit diagram for the temperature controller shown in Fig.3.3b.

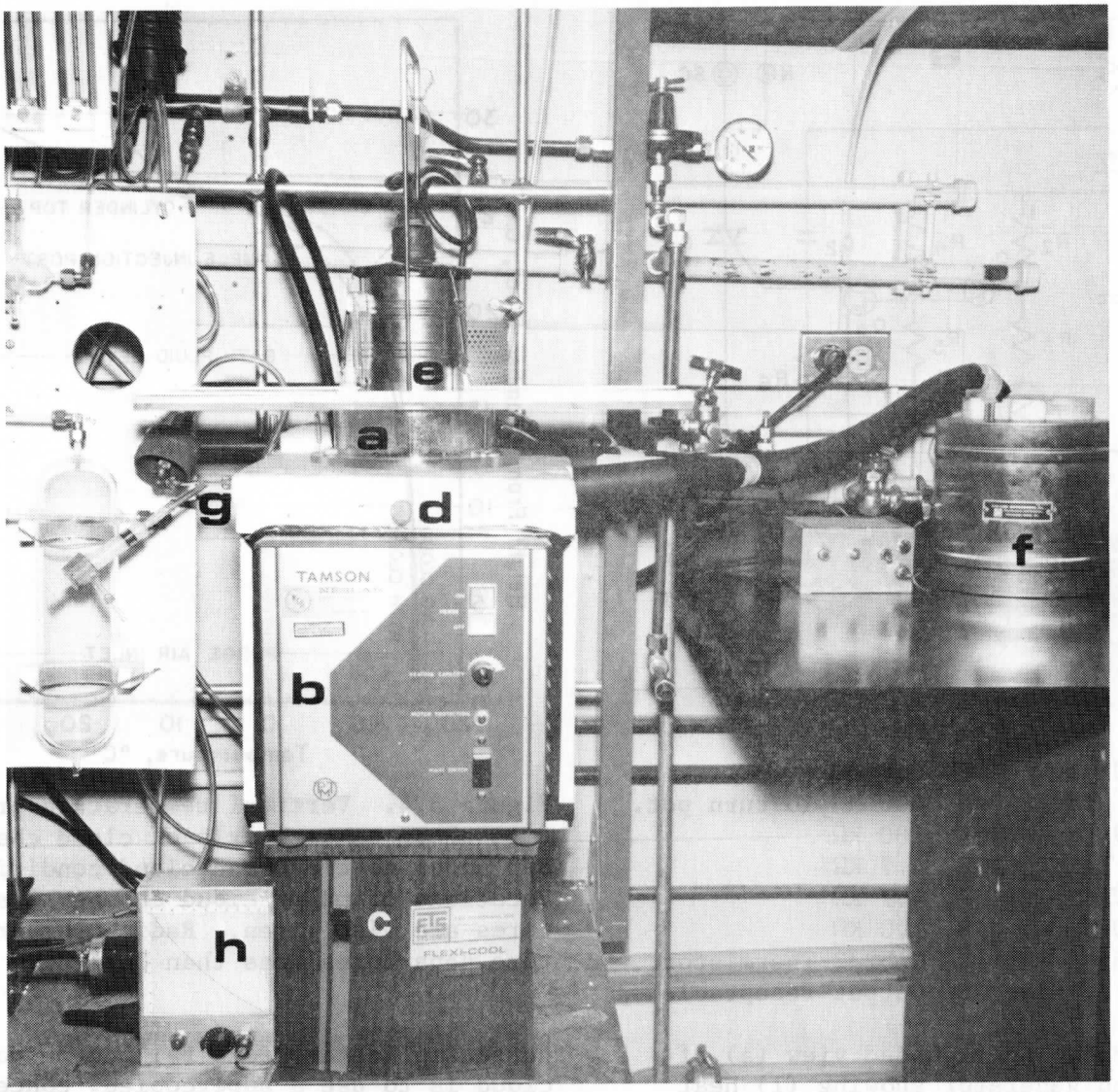

Fig. 3.2 A close-up of the cloud chamber (a) in operation showing constant temperature bath (b), refrigeration unit (c), sample injection port (d), cloud former (e) auxillarary heat exchanger (f), purge-air inlet (g), and cloud former temperature regulator (h).

3.5 Temperature distribution within chamber

An important premise in the interpretation of results based on the Ohtake style chamber is the existance of a nearly isothermal region within the cloud chamber. Temperature measurements with a copper-constant thermocouple, Kiethly Model 602 electrometer, and ice bath reference temperature were made on the chamber. Figure 3.4 shows the vertical profile of temperature along the axis of the chamber for both no-cloud and cloud conditions. Modification of temperature distribution under cloud conditions occurs mainly within the plexiglas collar due to the elevated temperature of the moisture supply. Radial temperature departures are less than 0.2 C throughout.

3.6 Frost prevention

A common problem in all sub-freezing cloud chambers is the formation of frost and frost splinters on the walls. Coating the walls of the chamber with

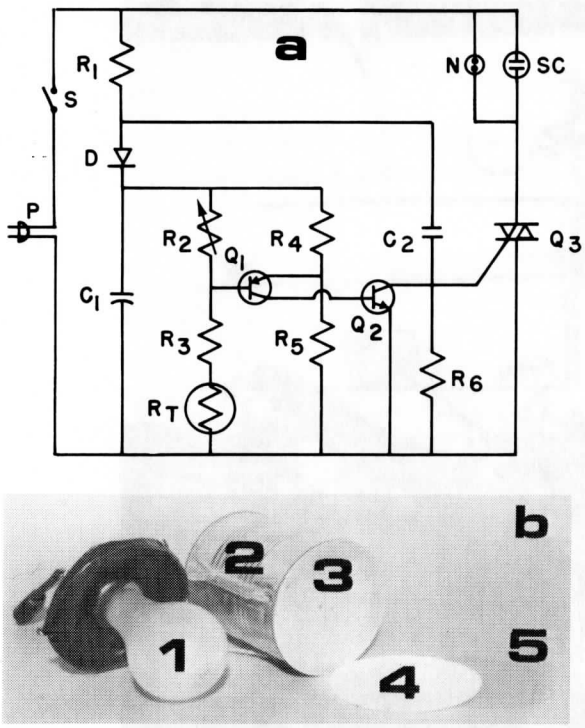

C_1	10μfd, 50V	R_1	6.8 KΩ
C_2	0.15 μfd	R_2	400 KΩ,10 turn pot.
D	IN649	R_3	100 KΩ
N	Neon lamp	R_4	4.7 KΩ
P	115 VAC plug	R_5	4.7 KΩ
Q_1	2N2907	R_6	1.0 KΩ
Q_2	HEP 55	R_T	GA52J2 Thermistor
Q_3	2N5573 Triac	SC	Output receptacle

Figure 3.3. An expanded view (a) of the cloud generator showing (1) heat source, (2) water reservoir, (3) bottom plate with holes for thermistor probe and water input, (4) filter paper pad, (5) support screen. In (b) the schematic for the zero-crossing electronic switch and parts is given.

glycerine or ethylene glycol is the usual approach to eliminating this problem. Our approach is no different.

A urethane foam roller saturated with glycerine presses against the inside of the chamber. Rods extending up through the top plate are used to run the roller up and down the wall before each ice nucleus measurement sequence is started.

3.7 Ice crystal detection

One of the simplest means of de-

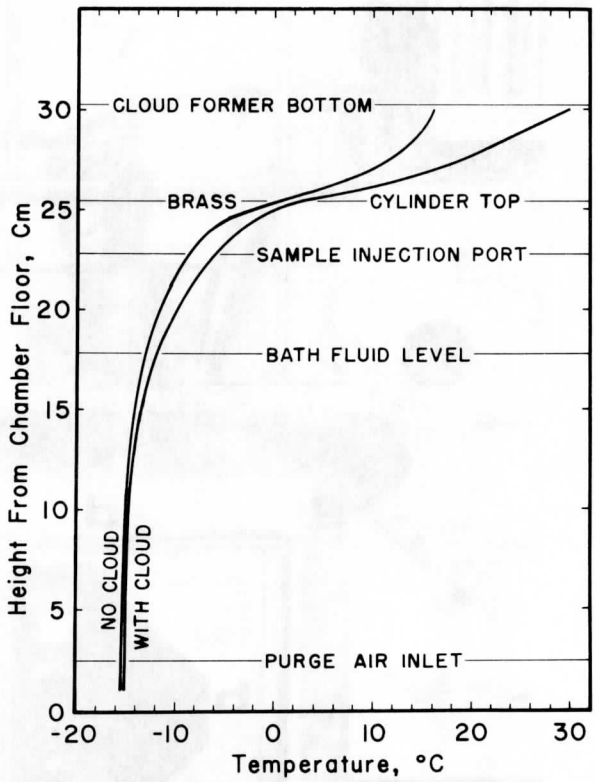

Figure 3.4. Vertical temperature profile along central axis of cloud chamber under no-cloud and cloud conditions. Locations of major cloud chamber features are also given. Radial temperature departures less than 0.2C.

detecting ice crystals falling out of a cloud is to use a supercooled, concentrated sugar solution in which ice crystals can grow to visible size. We have used this method since March of 1973 with considerable success.

The sugar solution is prepared by dissolving 360 gm pure cane sugar into 340 gm demineralized and filtered water; 25 cm^3 glycerine is added to the mixture. The hot solution is filtered through a 0.8 μm pore size membrane filter and allowed to cool. Gylerine is added to the solution to retard the rate of growth of the crystals. Approximately 10 cm^3 of the solution covers a 10 cm diameter petri dish with a layer ∿0.3mm deep. A fresh solution is used for each ice nucleus measurement.

3.8 Operation sequence

After a trial and error period

lasting several months the following procedural sequence was formulated that yielded consistent results. The selection of some of the time intervals is purely empirical; the events involved appear to run their course during the chosen intervals.

Prior to the start of an ice nucleus measurement the cloud chamber is brought to and maintained at the operating temperature of -16C. This temperature was selected because many ice nucleus measurements reported in the literature are also at this temperature. A continuous flow of specially dried air enters the bottom of the chamber. The bottom of a 10 cm diameter pyrex petri dish is covered with 10 cm^3 sugar solution; the petri dish is placed on the floor of the chamber. After the chamber lid is slid closed, the purge valve remains open for 5 minutes to allow the petri dish to cool to the chamber temperature and to purge the chamber of room air brought in with the petri dish. During this time water is usually added to the reservoir on the cloud generator to make sure the filter paper is saturated.

At the end of the 5 minutes the purge value is closed and the cloud generator is positioned over the chamber and is turned on. A second 5 minute period begins. Within 2 to 3 minutes small droplets can be seen falling within the plexiglass collar; their size is estimated to be less than 10 μm diameter. After 5 minutes the chamber appears full of cloud and the upper boundary of the cloud is clearly defined.

A sample of ice nucleus aerosol is now injected into the center of the cloud by inserting a thin glass tube through the injection port. Sample size may vary from 2 to 10 cm^3 depending on the activity of the aerosol. Within 30 seconds it is often possible to see the first crystals growing in the sugar solution. Crystals continue to settle into the solution for up to 10 minutes after the injection. Frequent visual checks of the number of crystals in the dish are made and the final number after 10 minutes is considered to be the total number of ice nuclei active in the sample injected.

Termination of the run is marked by opening the purge value, turning the cloud generator off and removing the ice covered petri dish. A period of approximately 10 minutes is allowed for the chamber to purge before the next run is started. It is possible to make one ice nucleus measurement every 30 minutes.

3.9 Crystal photography

Early in the operation of the system we made photographic records of ice crystal number in the petri dishes. One advantage of such a system was the possibility of crystal counting in which time is less of a factor. However, the design of the chamber did not lend itself to the easy removal of the petri dish for photographing, nor to photographing the dish within the chamber. We removed the dish from the chamber, positioned it in a specially built photostand, and took the picture.

Two approaches to crystal photography were taken. In one the crystals in the sugar solution were photographed in transmitted light. A small 12 watt sec electronic flash unit was positioned under a tray on which the petri dish rested. The camera, a Leica with 135 mm lens and extension bellows, was positioned above the dish. A cardboard truncated pyramid excluded room light and provided a dry and cool environment for the petri dish. An example of the photographs obtained with this technique is shown in Fig. 3.5a.

We found the contrast obtained with transmitted light and Plus-X film was not adequate for easy counting. The cardboard pyramid was modified to include diffuser windows of tracing paper and dual electronic flash lamps (Braun Hobby) were used to provide reflected light illumination. The results obtained with this approach are illustrated in Fig. 3.5b. Contrast is improved and crystal definition is also enhanced.

However, the inconvenience of removing the dish for photography, the film processing delay time and the repeated chore of manually counting the crystals led us to abandon the photographic approach to data acquisition

and rely on strictly manual counts of the number of crystals in the petri dishes. Of course, manual counting has its disadvantages, but provides real time information and must be done to some extent in any event.

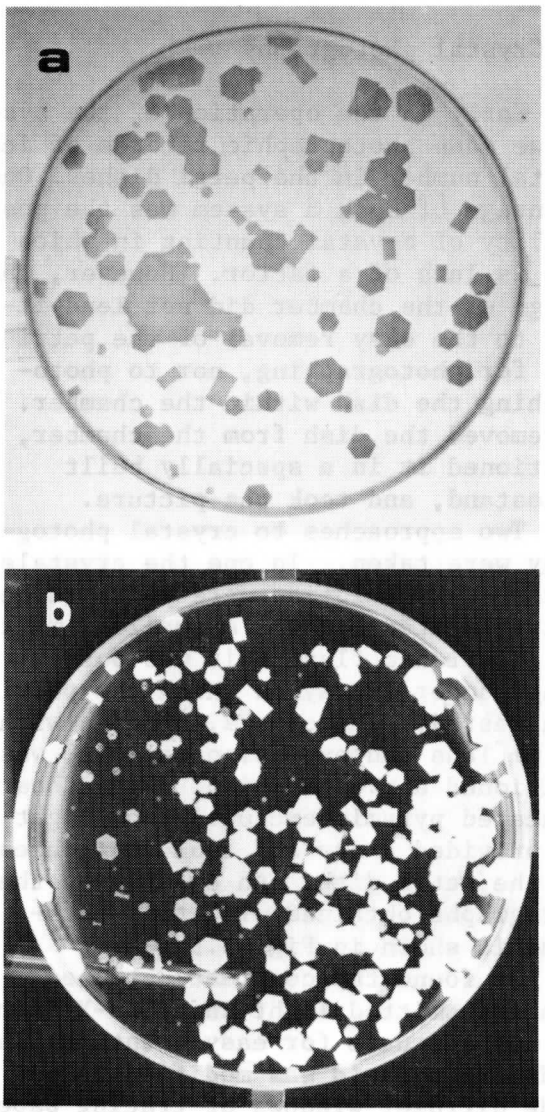

Figure 3.5. Photographs of crystals growing in sugar solution tray taken with (a) transmitted light and (b) reflected light. Improved contrast with reflected light makes this approach better suited to obtain photographic record of crystal number.

IV. Ice Nucleus Aerosol Source

Although any direct application of ice nucleus deactivation will involve natural ice nuclei we considered the use of a standard aerosol very important in trying to assess inhibition effects. We chose to use a thermally generated silver iodide aerosol. Aerosol generators involving the combustion of materials were not considered because of the possible interference of solvents and combustion products with the inhibition effects we sought. The remaining class of thermally produced aerosol may be grouped under hot wire or sublimation devices. Several approaches to hot wire aerosol generators were tried and abandoned. A major problem with most hot wire approaches is the nonuniformity of the powder coating placed on the heating element. We have circumvented this feature with a unique approach to hot wire production of silver iodide aerosols.

4.1 Preliminary hot-wire devices

During the development stages of this research several approaches to the thermal generation of silver iodide aerosols were tried. Our original design was based on a desire to eliminate contamination from external sources as much as possible. To this end we attempted to heat silver iodide powder in a pyrex glass tube. Nichrome heating wire wrapped around the outside of the tube provided the heat but the production of aerosol was meager. Only at temperatures above the softening point of the glass did aerosol generation begin.

As an alternative we used the sublimation of powder directly deposited on the heating wire as the aerosol source. Coating of the heating wire was done by sprinkling powdered silver iodide onto a hot element and allowing the powder to melt and fuse to the wire.

The performance of such a hot wire device was monitored via the interrelationships between drive voltage, total aerosol concentration, and ice nucleus concentration. We found a very pronounced time dependence of aerosol concentration. O'Connor and Roddy (1966) reported that platinum hot wire aerosol output shows a time variation until the temperature exceeds a critical value. Since silver

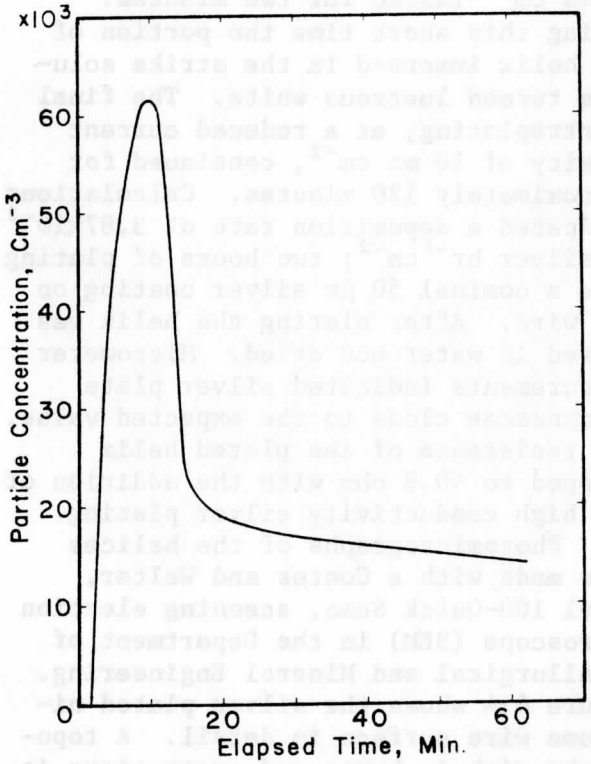

Figure 4.1. Time variation of aerosol output from AgI powder coated hot wire generator at 2.3 volts with aerosol output diluted 1:10 with clean air.

iodide is a much more volatile material, we excepted to also see such a temporal variation but at lower temperatures. We were unable however, to determine the critical temperature above which aerosol output remained constant for the powder coated hot wire. Figure 4.1 demonstrates the time variability of aerosol generation with the powder coated hot wire. Similar curves were obtained at other drive voltages. At times the output aerosol concentration would undergo orders of magnitude variations over short time intervals. This variability appears associated with nonuniform coverage of the filament by the powder. The necessity for frequent recoating compounded the problem of output variability. Output aerosol concentration was quite sensitive to the voltage applied to the heating element. Figure 4.2 shows a typical variation of aerosol concentration with voltage after 15 minutes of operation at that voltage.

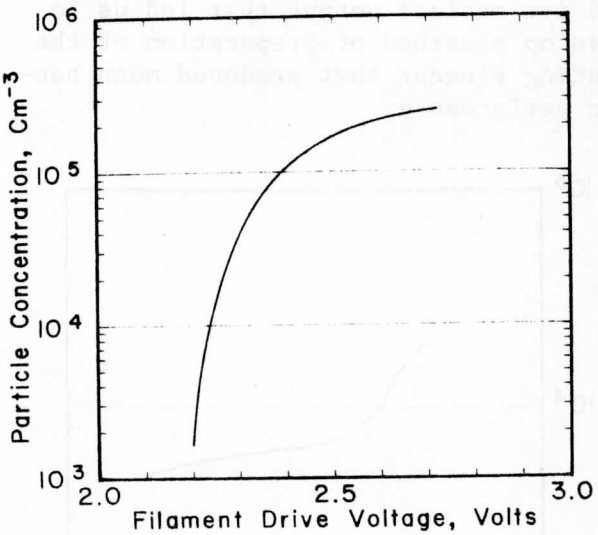

Figure 4.2. Aerosol output from AgI powder coated hot wire generator is very sensitive to filament drive voltage. Output measured after 1:20 dilution with clean air with Gardner counter in #4 detent.

Aerosol concentrations were measured with a Gardner model CN particle counter. This device allows for some coarse sizing of particles. The resulting cumulative size distribution is shown in Figure 4.3. It is quite apparent the greatest number of particles lies in the submicron range. This size distribution must be interpreted with caution. Not all condensation nuclei activated at the highest supersaturations produced in the Gardner counter may be silver iodide particles. Hot wires, especially when operated in air, yield a variety of products capable of acting as condensation nuclei at high supersaturation. Even so it is clear that a very big jump in concentration occurs at particles sizes smaller than 5×10^{-7} cm radius.

Along with the tremendous variability of aerosol concentration we found a large variability in the observed ice nucleus concentration as well. These fluctuations appeared to be correlated to fluctuations of total aerosol. The limited sample of aerosol concentration measurements with corresponding ice nucleus measurements was insufficient for a graphical presentation of results for this technique.

It was the variability of aerosol and ice nucleus output that led us to develop a method of preparation of the heating element that produced much better performance.

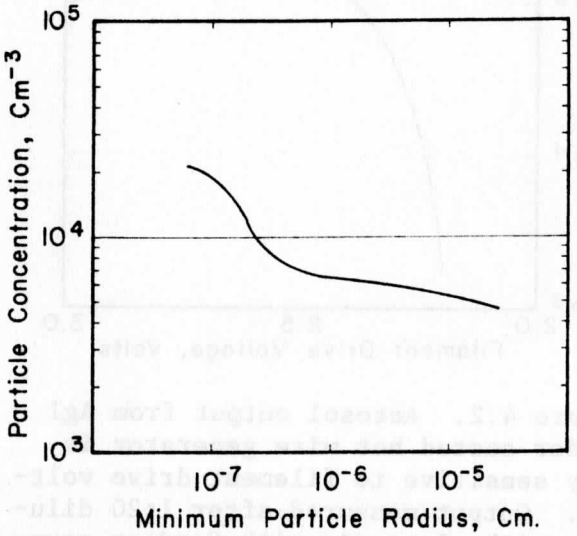

Figure 4.3. Cumulative size distribution of AgI powder coated hot-wire aerosol output obtained by varying expansion ratio on Gardner counter.

4.2 The Silver Iodide plated generator

The underlying concept in this technique is to bond a uniform layer of silver iodide to the heating element by electrochemical means. Silver plating the nichrome heating wire is the first step in this processes.

Standard silver plating techniques for nickel alloys were used. A strike solution was prepared containing 0.6 gm silver cyanide (AgCN) and 12 gm potassium cyanide (KCN) in 150 ml water. The standard plating solution consisted of 5.4 gm AgCN, 9.0 gm KCN, and 2.25 gm potassium carbonate (K_2CO_3) in 150 ml water.

A 20 cm length of 0.635 mm diameter nichrome wire was wound into a 6 to 8 turn helix 1.2 cm in diameter and approximately 3 cm long. The resistance of the untreated helix is nonimally 2 ohms. Before plating the wire is cleaned in an acid bath followed by a thorough wash in demineralized water.

Initial strike plating at a potential of 0.5 volts and current density of 20 ma cm^{-2} lasted for two minutes. During this short time the portion of the helix immersed in the strike solution turned lustrous white. The final electroplating, at a reduced current density of 10 ma cm^{-2}, continued for approximately 120 minutes. Calculations indicated a deposition rate of 3.87×10^{-3} cm silver hr^{-1}cm^{-2}; two hours of plating gave a nominal 50 μm silver coating on the wire. After plating the helix was rinsed in water and dried. Micrometer measurements indicated silver plate thicknesses close to the expected value. The resistance of the plated helix dropped to <0.8 ohm with the addition of the high conductivity silver plating.

Photomicrographs of the helices were made with a Coates and Welter, Model 100-Quick Scan, scanning election microscope (SEM) in the Department of Metallurgical and Mineral Engineering. Figure 4.4 shows the silver plated nichrome wire surface in detail. A topography rich in bumps and protrusions is readily apparent for the silver plate.

An approach similar to that used by Corrin et al. (1967) to prepare pure silver iodide was used to convert the silver plating into a coating of silver iodide. Each helix was weighed before and after plating to determine the mass of silver deposited. The helix and an amount of reagent grade iodine crystals equalling 90% of the stoichiometric mass for the formation of silver iodide were placed in a small pyrex ampule. The ampule was evacuated while cooled at dry ice-acetone temperature and sealed after 15 minutes of pumping with a mechanical pump.

During this mild exposure to iodine vapor the helix became a dull purple-violet with reds, greens and blues appearing as the initial reaction progressed. All ampules were baked at 155°C for a minimum of 24 hours. Shortly after the ampules were in the oven the vials were filled with bright purple iodine vapor. However, at the end of the reaction period in all ampules with a stoichiometric deficiency of iodine no trace of iodine crystals or vapor could be seen.

Most of the helices so treated

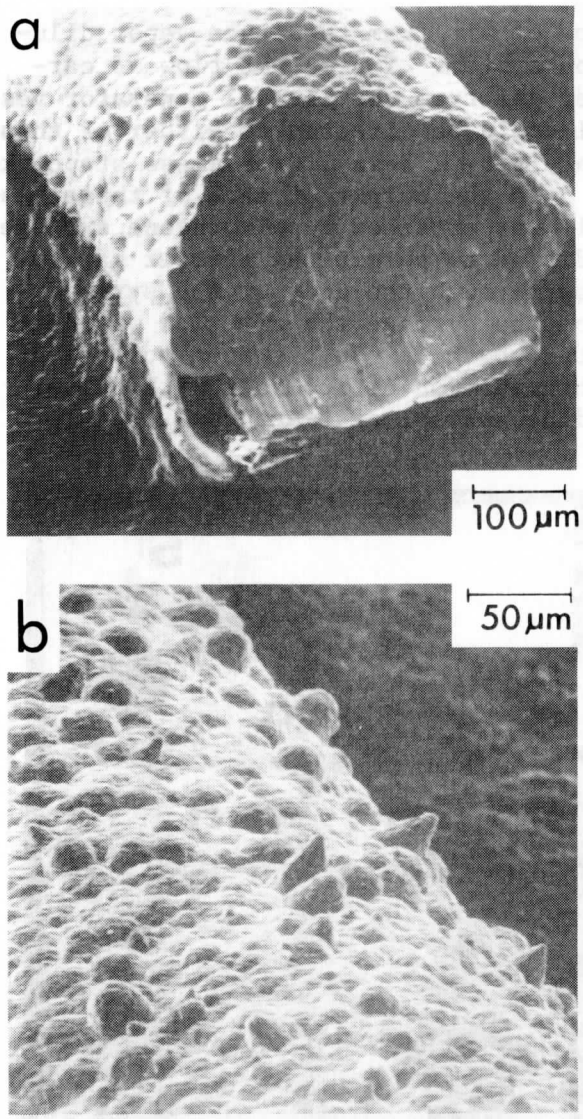

Figure 4.4. S.E.M. photomicrographs of surface of silver plated nichrome wire. In (a) the cross-section of the wire and thickness of plated silver layer can be seen. A close-up of the surface in (b) reveals a very rough topography.

have a dark yellow-purple surface. Only near the ends of the silver plated portion does the coating have the characteristic yellow silver iodide color. Perhaps in these areas iodine molecules are able to migrate along the silver-nichrome interface. The thickness of the silver iodide coating is substantially greater than the silver plate as one would expect from the difference in density between these two substances and the incorporation of the additional iodine mass in the layer. The resistance of the heating element after treatment with iodine vapor returned to nearly the pre-silver plate value in all cases.

The photomicrographs of Fig. 4.5 illustrate the remarkable change in surface texture that was brought about by the conversion to silver iodide. Here too, the increase in thickness of the coating can be seen.

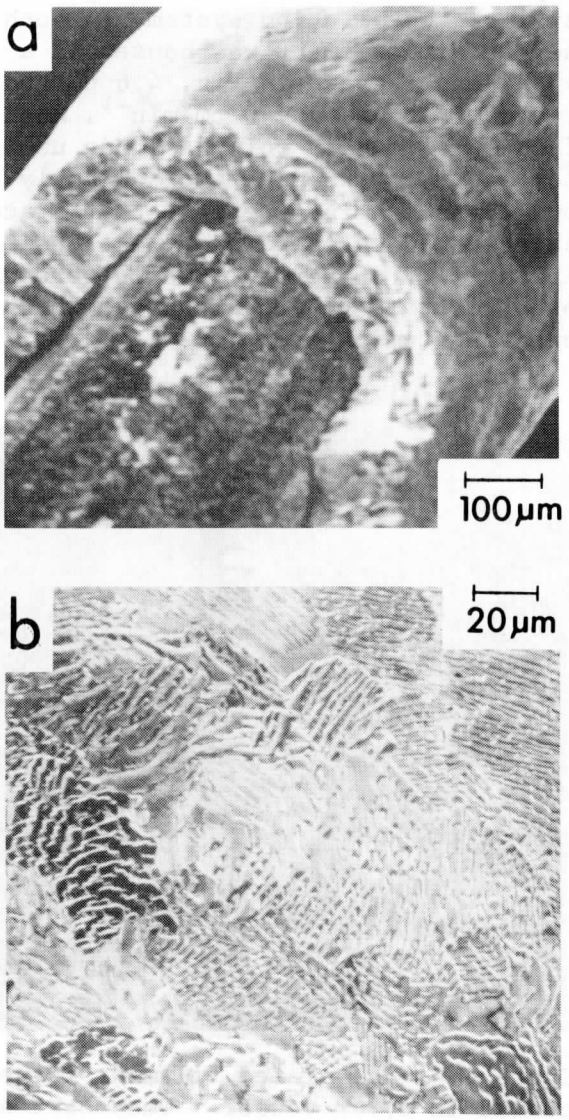

Figure 4.5. S.E.M. photomicrograph of surface of plated michrome wire after reaction with iodine vapor. On (a) the increased thickness of the plated layer is seen. A close-up of the surface in (b) shows the bumps and protrusions seen in Figure 4.4b are replaced by a smooth, lamellar surface.

The bumps and protrusions of the silver plate have given way to a smooth lamellar surface. This surface may be composed of the growth faces of individual crystals forming a polycrystalline coating on the wire.

4.3 The aerosol generator system

Two approaches were followed to incorporate the hot wire aerosol generator into the dilution system. In both the hot wire element was housed in a pyrex vessel shown in Fig. 4.6 purged by a carrier gas at 40 $cm^3 min^{-1}$. Much of our preliminary work was done using the output of the generator directly. However to examine the effect of trace gases we had to compare the ice nucleating ability of aerosols which were exposed to trace vapors and those which were uncontaminated.

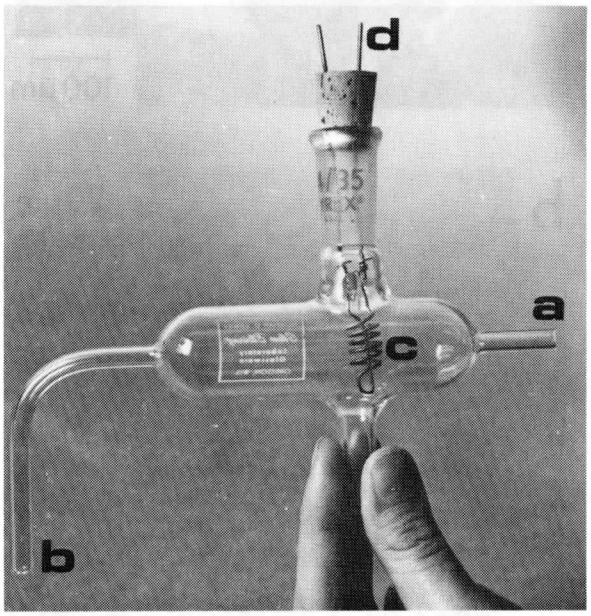

Figure 4.6. AgI plated filament is seen mounted in pyrex vessel. Quenchant air flow enters at (a) and carries aerosol out at (b). Nichrome helix (c) is crimp fastened to copper leads (d) through cork.

The first setup to do this consisted of two large pyrex glass mixing vessels as shown in Fig. 4.7. One received a flow of clean dry air as a diluent, the other received an equal flow of air from the trace vapor dilution system. The output flow of carrier gas from the aerosol generator vessel could be directed to either of these vessels by a 3-way, greaseless stopcock.

To the output of each of these vessels was attached a polyethyene syringe modified to permit the carrier gas to flow through the body of the syringe. From the syringe the air flow was directed to the exhaust system to prevent contamination of room air with silver iodide aerosol or trace vapors.

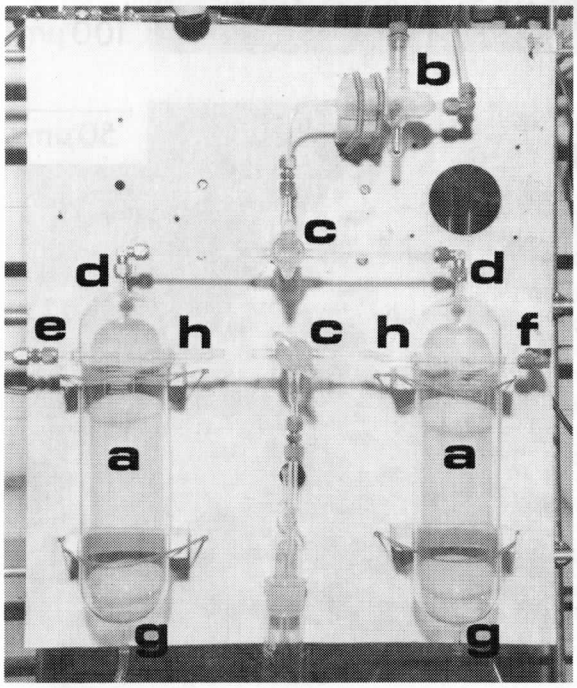

Figure 4.7. Final mixing vessel panel: (a) 1065 ml pyrex vessels (b) aerosol generator, (c) 3-way stopcocks, (d) aerosol inlets, (e) clean air inlet, (f) trace vapor inlet, (g) outlets, (h) spare inlets.

This approach was used with good success. The volume of the glass mixing flasks at the flow rates used resulted in a residence time of approximately 30 seconds. At very low concentrations of trace vapor, however, we were concerned that the aerosol particles may not have sufficient time to absorb the vapor. Therefore we modified the system to include much larger mixing vessels.

Our new mixing vessels were each

made of two large polyethyene trash bags sealed together at the opening. Appropriate inlet and outlet plumbing was attached. The inflated volume of each bag is estimated to be 300 liters, giving a residence time of more than 2.5 hours at the flow rates we used.

The output of the aerosol generator was directed to each bag through a 3-way solenoid valve. Each bag receives the full generator output during alternate three minute intervals. As is seen in Fig. 4.8, the long residence time serves to smooth out the step function input of aerosol to each bag as well as short term fluctations of aerosol output by the generator. The input plumbing contains a diffuser to prevent streaming of the carrier flow through the bag and also helps to provide thorough mixing within each bag. As before, the output of each bag passes through a sampling syringe and then on the the exhaust line.

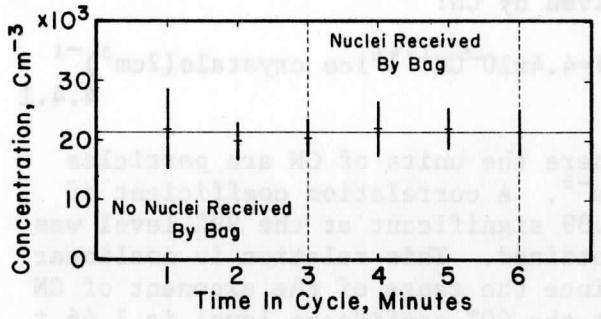

Figure 4.8. Aerosol concentration within large polyethylene mixing bag given as a function of time within the six minute cycle interval. Step function input to bag effectively smoothed by 2.5 hour residence time.

An important part of the aerosol generator system is the power supply to drive the heating element. This item also underwent several modifications. A voltage of less than 6 volts at less than 2 amps produced adequate heating of the nichrome wire heating elements to vaporize the silver iodide and produce an aerosol. It was necessary to control and stabilize the drive voltage to maintain a constant output of aerosol.

Our first approach was to reduce and regulate AC line voltage with a Variac and use a 6.3 volt filament transformer to reduce the voltage to the final value. Fluctuation of line voltage was a problem so we then used a surplus Sola constant voltage transformer to provide a stable 6.3 volt output. The heating element was then connected to the output of a Variac which provided control of the applied voltage. Though simple, this approach has proven satisfactory. The voltage and current are normally monitored when the generator is in operation.

4.4 Performance of plated hot wire aerosol source.

The performance of the silver iodide plated aerosol generator was monitored in terms of the power disipated by the helix, the total aerosol number as measured by the Gardner counter, and the number of ice crystals produced in the cloud chamber at -16C as counted in the sugar solution. We found the total aerosol count to behave as is usually expected of a hot wire aerosol source. Transient output of the plated helix source occurs at low power dissipations, however, at power dissipations in excess of ∿6 watts a permanent output lasting for several weeks was found.

Several parameters are known to affect the output of a hot wire aerosol source. The temperature of the filament is an important factor but was not directly measured in our system. Instead the power dissipated by the helix was determined from the voltage and current measurements at hand. Helix temperature is a function of power dissipation and also of the rate of quenchant air flow over the helix. The quenchant flow also affects the number and size of aerosol produced by affecting the local supersaturation of the vaporized silver iodide components. For these reasons we chose to retain a constant quenchant flow rate for our experiment of 40 $cm^3 min^{-1}$; no attempt was made to determine the dependence of aerosol number on quenchant flow rate. The dependence of total aerosol output on the power dissipation by the helix is shown in Fig. 4.9.

During our initial measurements with powder coated hot wires we noticed a decay in the generator output over a period of several hours. To obtain a

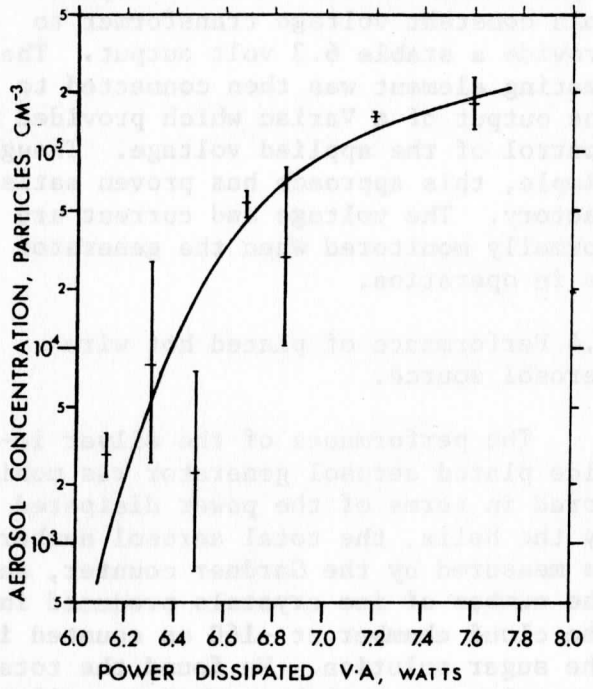

Figure 4.9. Aerosol output is shown to depend on power dissipated by helix at a constant quenchant rate of 40 cm min^{-1} and after a 2:25 dilution with clean air. Vertical error bars give standard deviation of the response shown by several different helices at different ages to the power dissipated.

consistant output of both total particle concentration and ice crystal concentration, we tried a procedure in which the generator is turned on approximately 10 minutes before sampling and shut off immediately after sampling. Even with this approach we noted a decay in output after several days of operation. Our present procedure with the plated filament is to heat the filament continuously. As is seen in Fig. 4.10 the output remains essentially constant for several weeks. Eventually the output decays, yet by periodically readjusting the power dissipation to produce the desired output of ice nuclei additional periods of stability can be achieved.

The relationship between total aerosol production and ice nucleus activity of the aerosol produced by the plated aerosol generator is shown in Fig. 4.11. These measurements were made with the cloud chamber at -16C and the moisture source at 42C. A least squares

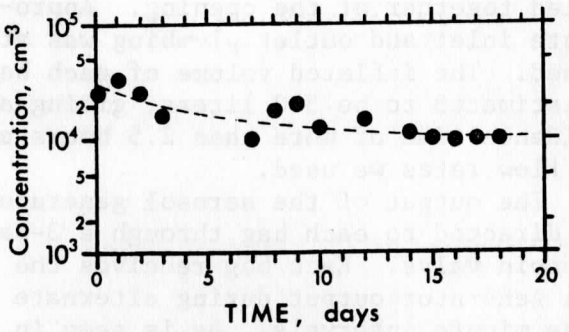

Figure 4.10. The long term output stability from a plated helix at constant power dissipation is shown here over a period of 20 days.

best fit straight line yields the following relation expressing the number of crystals (IN) observed in the sugar solution from a 2 cm^3 aerosol sample with a total aerosol concentration given by CN:

$$IN = 4.4 \times 10^{-5} CN^{1.46} \text{ ice crystals} (2 cm^3)^{-1} \qquad 4.4.1$$

where the units of CN are particles cm^{-3}. A correlation coefficient of 0.89 significant at the 99% level was obtained. This relation is nonlinear since the range of the exponent of CN at the 90% confidence level is 1.46 ± 0.23. This nonlinear response of ice nucleus to total aerosol concentration is a result of changes in the size distribution of the aerosol as its concentration increases.

We have found crystal numbers in excess of 100 difficult to count because of crystal overgrowth in the sugar solution. Also, crystal counts less than 20 do not provide a statistically significant number, especially when changes in crystal count are sought.

Size distribution measurements on the undiluted aerosol leaving the generator housing, were made by collecting a sample of aerosol in a thermal precipitator and observing the deposit on a scanning electron microscope. A series of photomicrographs of the thermal precipitator sample were analysed to obtain a size distribution of the

aerosol. The size distribution obtained is shown as a histogram in Fig. 4.12. Resolution limitations on the photomicrographs prevented counting of particles smaller than 0.1 μm diameter. Minor corrections, shown as a hatched band on the histogram, were applied to account for diffusional losses during sampling. The photomicrographs obtained show a large number of particles in excess 1.0 μm diameter.

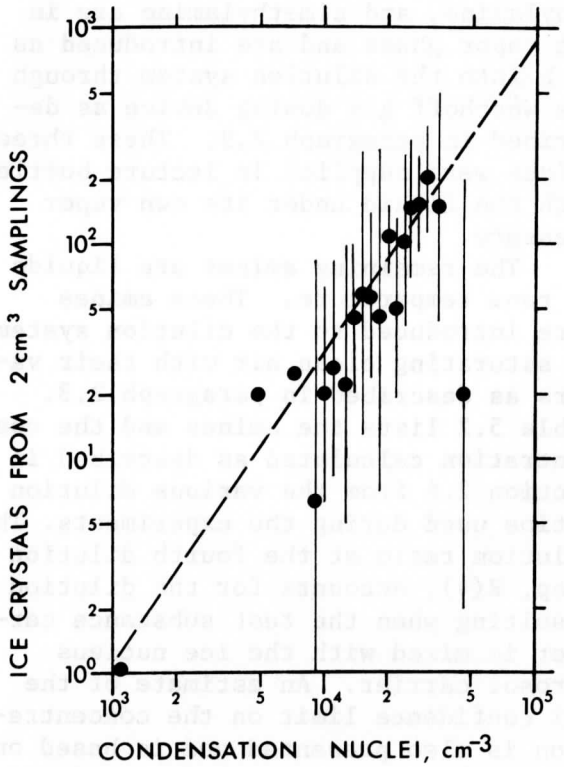

Figure 4.11. Correlation between aerosol concentration and observed ice crystal count from 2 cm^3 samples is seen to be high and have a slope slightly greater than 1:1. Vertical bars give standard deviation of crystal count from several helices for similar aerosol concentrations.

In order to expand our information on the number and size of particles produced a log-normal density function of the following form was fitted to our data:

$$N(\Delta \ell nd)^{-1} = A\sigma^{-1}(2\pi)^{-\frac{1}{2}} \exp[-(\ell nc-\mu)^2/2\sigma^2] \qquad 4.4.2$$

where N is the number of particles observed in the interval $\Delta \ell nd$ centered on ℓnd, A is a normalizing constant; μ is the mean of ℓnd and σ^2 is the variance of ℓnd. A parabolic least squares fit with a multiple correlation coefficient of 0.95 significant at the 99.9% confidence level yielded the following values:

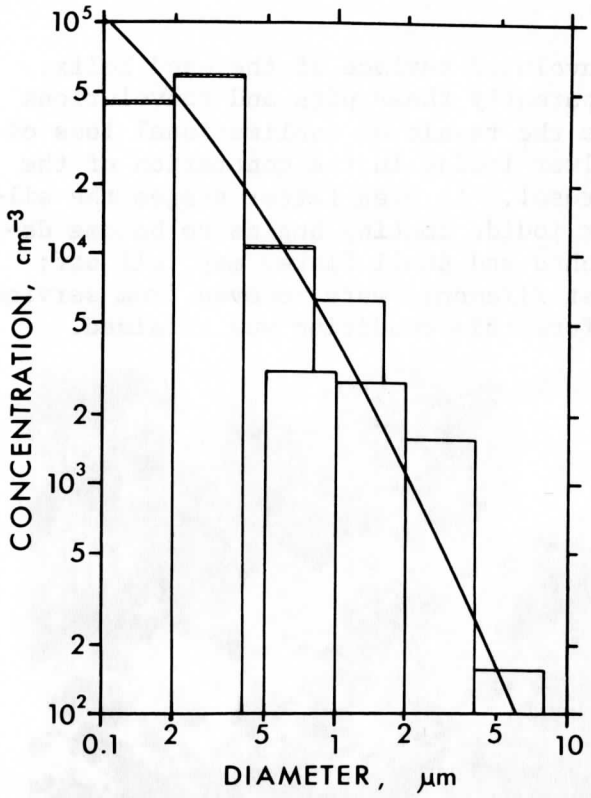

Figure 4.12. Aerosol particle size histogram based on S.E.M. photomicrographs of thermal precipitator deposit from output directly from AgI plated helix. Hatched band represents correction for diffusional losses. Solid curve is cumulative size distribution based on log-normal density function.

$$A = 1.1 \times 10^6 \text{ particles cm}^{-3},$$

$$\mu = -r.552 \text{ , and } \sigma = 2.936.$$

Based on μ the mean particle diameter is 0.011 μm. A cummulative size distribution which gives the number of particles with a larger diameter is given as the solid curve in Fig. 4.12.

After several days of continuous operation the smooth lamellar surface of a new helix becomes deeply pitted. The photomicrograph in Fig. 4.13 shows the

convoluted surface of the used helix. Apparently these pits and convolutions are the result of sublimational loss of silver iodide in the generation of the aerosol. At even latter stages the silver iodide coating begins to become detached and small flakes may fall off; most filaments were removed from service before this condition was attained.

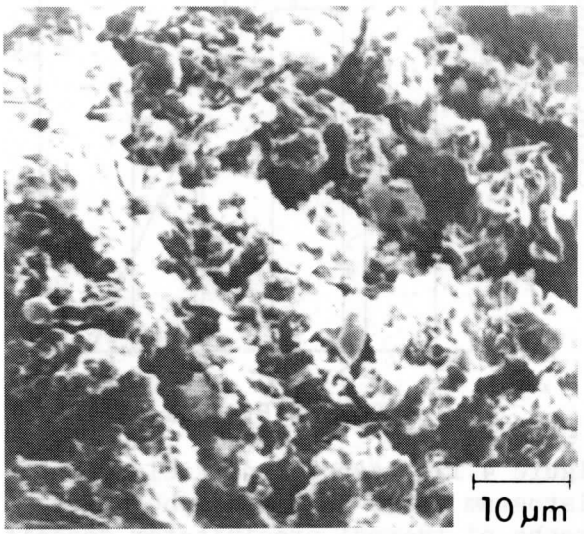

Figure 4.13. S.E.M. photomicrograph of the surface of an old AgI plated filament. Deep pits and convolutions reflect material lost in process of aerosol generation.

V. Ice Nucleation Inhibition by the Amines

The effect eleven amines have on the ice nucleating ability of silver iodide aerosols was examined in the course of our research. Several of these amines were normal monoamines, while others were nitrogen containing organics from the large and diverse amine family. The normal amines consisted of a sequence of six primary amines from methylamine through dodecylamine spanning a molecular weight range from 31.06 to 185.35. The second group included one di-amine, three amines with nitrogen incorporated in a ring structure, and one aromatic amine. This diversity of compounds tested provides a cross section of the behavior of the amines as ice nucleus inhibitors within the context of the experiments herein described. A list of the amine compounds investigated is found in Table 5.1 in which the physical properties of these amines are presented. The vapor pressure data is discussed in Appendix I.

5.1 Amines in the dilution system

The amines investigated exist as liquids or vapors at normal room temperature and pressure. Methylamine, ethylamine, and dimethylamine are in the vapor phase and are introduced as such into the dilution system through the Wösthoff gas dosing device as described in paragraph 2.9. These three amines were supplied in lecture bottles with the liquid under its own vapor pressure.

The remaining amines are liquids at room temperature. These amines were introduced to the dilution system by saturating clean air with their vapors as described in paragraph 2.8. Table 5.2 lists the amines and the concentration calculated as described in section 2.6 from the various dilution ratios used during the experiments. The dilution ratio at the fourth dilution step, R(4), accounts for the dilution resulting when the test substance carrier is mixed with the ice nucleus aerosol carrier. An estimate of the 90% confidence limit on the concentration is also presented and is based on the error analysis given in sections 2.6, 2.7, and 2.8. All flowrates are considered accurate to 5%. Our knowledge of ambient atmospheric pressure is considered accurate to 5%. We estimate the accuracy of the saturation vapor pressure assigned to the last bubbler to be 10%. This value is based on a ± 1C° standard deviation of the bubbler temperature and knowledge of B in eq. 2.8.2 (see Appendix I for details). All estimates of relative error are conservative figures to insure that our error estimate marks the outer bounds. The computer program used to calculate the concentration is given in Appendix II. All concentration computations assume uniform mixing, equilibrium of wall losses or gains, and no sinks for the test substance in the system.

Table 5.1 Physical properties of selected amines

Compound	Structural Formula	Molecular Weight	Density gm/ml	Freezing Point C	Boiling Point C	P_{oc} mb	P_{20c} mb
Methylamine (n)	CH_3NH_2	31.06	$0.7691^{-\frac{70}{4}}$	-92.5	- 6.5	1341	2904
Ethylamine (n)	$CH_3CH_2NH_2$	45.08	$0.7059^{\frac{0}{4}}$	-80.6	16.6	482	1108
Butylamine (n)	$CH_3(CH_2)_3NH_2$	73.14	0.7401	-50.5	77.8	31.2	94.2
Hexylamine (n)	$CH_3(CH_2)_5NH_2$	101.19	0.7675	-19.0	132.7	2.24	8.72
Octylamine (n)	$CH_3(CH_2)_7NH_2$	129.24	0.07769		179.6	.190	.920
Dodecylamine (n)	$CH_3(CH_2)_{11}NH_2$	185.35		27.5	259.1	.0019	.013
Dimethylamine	$(CH_3)_2NH$	45.08	0.6804	-96.0	7.4	730	1656
Morpholine	$O\ CH_2CH_2N\ CH_2CH_2$	87.12	0.9998	- 4.9	128.9	7.77	13.84
Pyridine	$N{:}CH\ CH{:}CH\ CH{:}CH$	79.10	0.982	-42.0	115.3	5.37	19.4
2,4 Lutidine	$N{:}\ C(CH_3)CH{:}C(CH_3)CH$	107.15	0.9493		157.1	.872	3.48
Benzylamine	$[C_6H_5]CH_2NH_2$	107.15	0.9826		184.5	.133	.650

5.1.1 Physical effects on dilution system

Although most of the dilution system is made of pyrex glass which is uneffected by the amines some non-glass components did show the effects of prolonged exposure to the amines. Most noticeable was a yellowing of the Tygon (R3603) vinyl tubing connecting various points of the dilution system to the manometer manifold. Discoloration of this tubing occured rapidly at high amine concentrations and was less noticeable at reduced levels. Mayon (R220) vinyl tubing used in the air supply system and used to connect the final dilution vessel and the mixing vessels also showed signs of yellowing after continue exposure to the amine. Those sections of vinyl tubing which yellowed were frequently replaced to prevent interference from previously used amines.

Three of the amines, hexylamine, octyamine, and morpholine, introduced to the dilution system via the bubblers caused the lead (warm) bubbler to clog after varying periods of use. Apparently these amines reacted with a component of the carrier air stream to produce a solid precipitate that blocked the fritted glass bubble dispenser. We suspect that these amines combined with water and/or oxygen in the clean air supply to form a hydrate or oxide that was deposited in the glass frit. This deposit always formed in the lead bubbler, the second bubbler was unaffected indicating the interfering gas component was removed by the first bubbler. The clogged glass frits could be readily cleaned with water and reused. The problem was virtually eliminated by replacing the clean compressed air supply with a high purity, dry, bottled nitrogen supply. Eventually we expanded our use of dry nitrogen as the carrier gas to include the Wösthoff gas dosing device, silver iodide aerosol generator, and first dynamic dilution chamber as well as the bubbler train.

The readily identifiable and objectionable odor of the amines made leaks in the dilution system easy to diagnose. The most serious leak problems were encountered with the vaporous amines due to the high concentrations produced in the vicinity of the leaks.

Table 5.2 Concentration data for selected amines

Material	C	S90	PI	P	SF	FW	R(1)	R(2)	R(3)	R(4)
1.Methylamine	3.7-04	7.8-05	1.0+03	1010	10	500	4.0			0.018
2.Ethylamine	3.7-04	7.8-05	1.0+03	1010	10	500	4.0			0.018
3.Ethylamine	3.3-04	7.1-05	1.0+03	1010	10	500	4.5			0.015
4.Ethylamine	3.7-05	7.7-06	1.0+03	1010	1	500	4.0			0.018
5.Ethylamine	3.3-05	7.1-06	1.0+03	1010	1	500	4.5			0.015
6.Ethylamine	8.7-07	2.0-07	1.0+03	1010	1	500	210.			0.016
7.Ethylamine	9.1-10	3.4-10	1.0+03	1010	1	500	200.	1000.		0.016
8.Ethylamine	8.1-13	5.0-13	1.0+03	1010	1	500	1000.	200.	1000.	0.016
9.Butylamine	2.9-03	1.1-03	3.1+01	979	0	0	1000.			0.015
10.Butylamine	1.2-03	4.8-04	1.2+02	979	0	0	1000.			0.016
11.Butylamine	3.1-04	1.3-04	3.1+01	979	0	0	1000.			0.016
12.Hexylamine	2.3-04	8.8-05	2.2+00	980	0	0	9.0			0.016
13.Hexylamine	2.2-05	8.8-06	2.2+00	983	0	0	100.			0.016
14.Hexylamine	2.3-06	9.1-07	2.2+00	979	0	0	1000.			0.016
15.Octylamine	2.0-05	8.0-06	2.0-01	977	0	0	9.0			0.016
16.Octylamine	2.0-06	8.0-07	2.0-01	983	0	0	100.			0.016
17.Dodecylamine	1.3-07	5.2-08	1.3-03	977	0	0	8.0			0.016
18.Dimethylamine	3.7-04	7.8-05	1.0+03	1010	10	500	4.0			0.018
19.Morpholine	7.8-04	3.1-04	7.8+00	979	0	0	8.0			0.016
20.Pyridine	2.7-04	1.1-04	5.4+00	975	0	0	18.			0.020
21.Pyridine	1.1-04	4.3-05	5.4+00	964	0	0	48.			0.020
22.Pyridine	8.1-06	3.3-06	5.4+00	975	0	0	670.			0.020
23.Pyridine	9.9-07	5.8-07	5.4+00	979	0	0	100.	500.		0.020
24.2,4 Lutidine	3.5-05	1.4-05	3.5+00	969	0	0	100.			0.020
25.Benzylamine	1.3-05	5.2-06	1.3-01	987	0	0	9.0			0.020

C = concentration

S90 = 90% confidence interval on C

PI = Amine source vapor pressure (mb)

P = Ambient air pressure (mb)

SF = Wösthoff cycle frequency (min^{-1})

FW = Wösthoff diluent flowrate (cm min^{-1})

R(1,2,3)= Dilution ratio for dilution vessels

R(4) = Dilution ratio for final mixing vessel.

In these situations, moistened pink litmus paper, which rapidly turned blue when placed near the leak, could safely be used as a leak detector. Leaks of this type usually occurred at the lecture bottle connections to the Wösthoff gas dosing device. Leaks downstream of the dosing device and dilution vessels were not encountered with the glass aerosol-test gas mixing vessels. However, after we switched to the large polyethylene bag mixing vessels, we did notice a lingering presence of amine odor. We suspect, that amines permeate the thin polyethylene walls of these bags and contaminate the room.

5.1.2 Physiological effects

All the amines are bases which produce mild to severe irritation of eyes, skin, and mucous membranes through direct contact and are to varying degrees toxic when inhaled, ingested, or absorbed through the skin. We took the precaution of wearing gloves and working in a fume hood when filling the bubblers and during clean-up of the apparaturs between runs. However, as mentioned above the permeation losses through the bag walls allowed pyridine and 2, 4 lutidine to reach objectionable levels in the room. Even with the exhaust system in operation mild stomach upset and headaches were experienced by those working in the laboratory at the time. Of all the compounds dealt with in our study these two were the most objectionable. Table 5.3 gives a summarization of the physiological impact of the amines used here as found in Sax (1968). We are unable to say, for lack of an airborne amine concentration analysis technique, what concentration levels were present in the laboratory when we experienced discomfort. However, Oettel (1963) points out that while a concentration of pyridine or its derivatives is detectable at 1 ppm at 30 ppm it is intolerable to most people. Therefore the concentration of either pyridine or 2,4 lutidine which gave rise to our physical discomfort must have been less than the later value.

5.2 Experiment design

The hypothesis on which our experimental study of ice nucleation inhibition was based is that the ice nucleus aerosol treated with the test gas at a given concentration will yield a detectably smaller number of ice crystals in our cloud chamber than an equal sample of untreated aerosol. With only one cloud chamber we had to rely on sequential observations of ice nucleus activity and usually sought to alternate measurements on the treated and untreated aerosol. The inherent variability of ice nucleus concentration made it necessary for us to accumulate lengthly series of observations for some of the amines. In general a minimum of three pairs of measurements on the treated and untreated aerosol were obtained for each compound and concentration tested.

Our approach to the design of the experiment, while straight forward, has perhaps neglected some aspects of the statistical requirements for a sound experiment in which uncontrollable parameters introduce noise into the measurable results. In this regard, the variability of ice nucleus concentration presented the most serious difficulty. By a true randomization of the sequence of treated and untreated samples measured in the cloud chamber we could have had greater statistical confidence in our results.

5.3 Data analysis

The ice crystal count and condensation nucleus counts obtained in our experiment were divided into two groups. The first group included all those measurements obtained when the twin glass mixing vessels were used to combine the aerosol and test substance as described in the first part of section 4.3. With this arrangement the entire output of the aerosol generator is directed to one or the other mixing chamber to be combined with either a flow of clean air (untreated) or a flow of test substance at a given concentration in clean air (treated). Since all of the generator output entered each mixing vessel through essentially identical pathways all variability of ice nucleus concentration could be assigned to the nucleus source.

Table 5.3 Physiological impact of amines

	TLV[a] (ppm)	Toxicity[b] Acute	Chronic	Description
Methylamine	10	3	2	Strong irritant skin, eyes, mucous membranes.
Ethylamine	10	3	u	" "
Butylamine	5	2	u	Moderate irritant skin, eyes, mucous membranes.
Hexylamine	u	2	u	" "
Octylamine	u	1	u	Mild irritant skin, eyes, mucous membranes.
Dodecylamine	u	1	u	" "
Dimethylamine	10	2	u	Moderate irritant skin, eyes, mucous membranes.
Morpholine	20	2	u	Skin absorption, irritant skin, eyes mucous membranes.
Pyridine	5	1	2	Skin irritant, Central nervous system depressant.
2,4 Lutidine	5	1	2	" "
Benzylamine	u	3	2	Strong irritant skin, eyes, mucous membranes.

(a) TLV - Threshold Limit Value: condition to which all workers may be repeatedly exposed, day after day, without adverse effect.

(b) Toxicity rating code:

- 0 NONE : a) no harm under any condition; b) harmful only with overwhelming doses.
- 1 SLIGHT : Causes readily reversible changes, which disappear after exposure ends.
- 2 MODERATE : May involve both reversible and irreversible changes not severe enough to cause death or permanent injury.
- 3 HIGH : May cause death or permanent injury after very short exposure to small quantities.
- u UNKNOWN : No valid information for humans.

The situation is quite different in the second case in which we made use of the long residence time, polyethylene bag mixing vessels. In this situation the aerosol generator output is alternately directed from one bag to the other. Variations or inequalities in cycle period, tubing path length, and bag geometries introduced additional variations in ice nucleus concentration not assignable to the aerosol source. Hence the data obtained when this system of aerosol and test substance mixing was employed was dealt with separately.

5.3.1 Analysis of data from small mixing vessels.

At each concentration of a particular test substance a set of ice crystal counts for treated and untreated samples were selected and stratified according to date of observation and generator power dissipation from groups with the greatest possible homogeneity. Average values (μ) and the standard deviation (σ) of the ice crystal count were then computed for the untreated (μ_u, σ_u) and treated (μ_t, σ_t) aerosol for each set of measurements. Student's t-test was applied to test the significance of the difference between the means (μ_u and μ_t) for each set:

$$t = \frac{|\mu_t - \mu_u|}{\sqrt{\frac{1}{N_u}+\frac{1}{N_t}}\sqrt{\frac{(N_u-1)\sigma_u^2+(N_t-1)\sigma_t^2}{N_u+N_t-2}}} \qquad 5.3.1$$

where N_t and N_u are, respectively, the number of data points for the average ice crystal count for the treated and untreated aerosols with the number of degrees of freedom equal to $N_u + N_t - 2$. In addition, the ratio of the means (α) for each set was computed along with its standard deviation (σ_α):

$$\alpha = \frac{\mu_t}{\mu_u}$$

$$\text{and } \sigma_\alpha = \alpha\sqrt{\frac{1}{N_u}\left(\frac{\sigma_\mu}{\mu_u}\right)^2 + \frac{1}{N_t}\left(\frac{\sigma_t}{\mu_t}\right)^2} \qquad 5.3.2$$

5.3.2 Analysis of data from large, bag-type mixing vessels.

The ice crystals count data for treated and untreated samples obtained with the large polyethylene bag mixing vessels were analysed by two methods. The first method is described in section 5.3.1 in which it is assumed that all ice crystal count variability is associated with the aerosol generator. The second method incorporates the additional information of total aerosol count obtained along with the ice crystal count.

Shortly before or after the aerosol sample was injected into the cloud chamber a total aerosol count was made with a Gardner Type CN small particle counter. Some correspondence between the number of ice nuclei present in a sample and the number of condensation nuclei (aerosol) particles ought to exist. Our work on the performance of the plated hot wire aerosol generator suggested a power law form for this relationship. The effect of the test substance on the activity of the aerosol as an ice nucleant should be manifested as a difference in the relationship between ice crystal production and condensation nucleus count for the treated and for the untreated aerosol. A least squares power law regression was fitted to the ice crystal-condensation nucleus data for both the untreated and treated data:

$$IN = A\,CN^B \qquad 5.3.3$$

where IN and CN are defined in section 4.4 and A and B are the regression parameters. A transformation of variables to:

$$y = \ell n\ IN \quad \text{and} \quad x = \ell n\ CN \qquad 5.3.4$$

linearizes this expression to

$$y = a + Bx \qquad 5.3.5$$

where $a = \ell n\ A$. For a linear correlation coefficient of r the variances of the regression parameters are

$$\sigma_a^2 = (1-r^2)\left[\frac{N}{N-1}\left(\frac{\bar{x}}{\sigma_x}\right)^2 + 1\right]\sigma_y^2$$

$$\text{with } \sigma_A = A\sigma_a \qquad 5.3.6$$

and

$$\sigma_B^2 = \frac{N}{N-1}(1-r^2)\frac{\sigma_y^2}{\sigma_x^2} \qquad 5.3.7$$

where $\bar{x} = \overline{\ell nCN}$, $\sigma_x = \sigma_{\ell nCN}$, $\sigma_y = \sigma_{\ell nIN}$, and N is the number of data points on which the regression is based. The geometric mean value of the aerosol concentration CN is readily obtained:

$$\hat{CN} = e^{\bar{x}} \quad \text{and} \quad \sigma_{\hat{CN}} = \hat{CN}\frac{\sigma_{\bar{x}}}{\sqrt{N}} \qquad 5.3.8$$

The regression equations enable a comparison of potential ice crystal counts that is decoupled from differences in aerosol concentration in the untreated and treated cases. This decoupling is possible by selecting a single value (z) of the aerosol concentration based on the geometric mean

values for the two cases:

$$z = \sqrt{\hat{CN}_u \hat{CN}_t} \quad \text{and}$$

$$\sigma_z = \frac{z}{2} \sqrt{\frac{\sigma^2_{\hat{CNu}}}{\hat{CN}^2_u} \quad \frac{\sigma^2_{\hat{CNt}}}{\hat{CN}^2_t}} \qquad 5.3.9$$

where the subscripts u and t refer, respectively, to the untreated and treated aerosols, $\hat{CN}$ is the geometric mean aerosol concentration and $\sigma_{\hat{CN}}$ is its standard deviation determined from the data giving the regression parameters. Now, for the untreated and treated aerosol we can compute

$$IN^*_{u,t} = A_{u,t} Z^{B_{u,t}} \quad \text{and} \quad \sigma_{IN^*_{u,t}}$$

$$= IN^*_{u,t} \sqrt{\frac{\sigma^2_{Au,t}}{A^2_{u,t}} + B^2_{u,t} \frac{\sigma^2_z}{z^2} + (\ell nz)^2 \sigma^2_{Bu,t}} \qquad 5.3.10$$

where the * indicates this value of the ice crystal count is derived from the regression equation. IN^*_u and IN^*_t are thus based on the same, though fictitious aerosol concentration (z). The significance of the difference $(IN^*_u - IN^*_t)$ can be evaluated with Student's t-statistic for infinite degrees of freedom:

$$t_{u,t} = \frac{\left| IN^*_u - IN^*_t \right|}{\sqrt{\sigma^2_{INu}{}^* + \sigma^2_{INt}{}^*}} \qquad 5.3.11$$

A ratio $(\tilde{\alpha})$, equavalent to α defined by eq. 5.3.2, can be formed of the two regression based ice crystal counts:

$$\tilde{\alpha} = \frac{IN^*_t}{IN^*_u} \quad \text{and}$$

$$\sigma_{\tilde{\alpha}} = \tilde{\alpha} \sqrt{\left(\frac{\sigma_{INu}{}^*}{IN^*_u}\right)^2 + \left(\frac{\sigma_{INt}{}^*}{IN^*_t}\right)^2} \qquad 5.3.12$$

The value of $\tilde{\alpha}$ obtained by this procedure can then be compared to the α obtained by the methods of section 5.3.1.

In addition to the power law ice crystal versus condensation nucleus concentration analysis we also examined the difference in condensation nucleus concentration between the treated and untreated aerosol. As previously discussed, any difference here could be attributable to configurational differences between the two aerosol mixing vessels. Of course, it is also possible that the test substance influences the condensation behavior of silver iodide aerosols as well. The mean value and standard deviation of the condensation nucleus concentration were computed for the treated and untreated aerosol. A ratio (β) analagous to that determined for the ice crystal counts was calculated for the condensation nucleus concentration along with the appropriate standard deviation and Student's t-statistic.

5.4 Results of amine ice nucleus inhibition

The experimental data for eight amines were analysed via the method discussed in section 5.3.1; four amines were dealt with as described in section 5.3.2. These data are presented in Table 5.4 and 5.5, respectively. Ice crystal count values, obtained at -16C from 2 cm^3 samples, represent averages based on the data of that group. In those cases where several days of data were available all the data were also combined into a single large data set. Combining all the data for a given amine and concentration resulted in an increase in degrees of freedom which, on comparing data from treated and untreated samples, far offset the usual increase of the standard deviation. It is for this reason the t-statistic and ratio α based only on the combined data are presented in Tables 5.4 and 5.5.

Each amine was not examined over the same range of concentration. If the amine proved only slightly effective at a relatively large (10^{-4}) concentration, we did not pursue inhibition by that amine at lower concentrations. For this reason methylamine, dodecylamine, dimethylamine, morpholine, 2.4 lutidine, and benzylamine

dodecylamine, dimethylamine, morpholine, 2.4 lutidine, and benzylamine were examined at only one concentration.

Ethylamine received considerable attention because it had been studied by other investigators as a nucleant suppressant and also used in the field. We extended our measurements to very low concentrations to try to duplicate the concentrations likely to be produced in the atmosphere by dispersal from an airplane.

Butylamine, hexylamine, octylamine and pyridine were examined at multiple concentrations because of their initial and persistent effectiveness in suppressing ice nuclei. In most of these instances, however, extreme low concentration effectiveness was not determined. We surmised a continuation of the observed trend as concentration decreased and concluded very low concentrations would yield little, if any, significant inhibition.

The data of Tables 5.2, 5.4, and 5.5 were combined to yield Fig. 5.1. The horizontal scale gives the logarithm of the amine concentration; each hash mark represents a factor of ten change in the concentration. Horizontal bars give the 90 percent confidence interval on the concentration based on our error analysis. The vertical scale is the ratio α, defined by eq. 5.3.2, presented in logarithmic fashion. The vertical bars give a 90% confidence interval on the value of α. Confidence limits on a logarithmic scale were calculated using the t-statistic scaling factor, t_{90}, for the appropriate degrees of freedom and the mean ($\bar{x}$) and standard deviation ($\sigma_{\bar{x}}$) for the parameter, i.e.,

$$x_{\substack{\max \\ \min}} = \bar{x} \exp\left[\pm \frac{t_{90}\sigma_{\bar{x}}}{\bar{x}}\right] \qquad 5.4.1$$

5.4.1 Results for primary amines

All the primary amines were tested with the dual glass final mixing vessels and data analysed by methods of section 5.3.1.

Methylamine. Based on the early work by Birstein (1957) with this amine we expected to see much better performance as an inhibitor than we observed in our experiment. The concentration of 3.7×10^{-4} was the highest we felt could be conveniently produced using the Wösthoff dosing device; yet only a 20% reduction in active nuclei was obtained. Birstein reported ice crystal production by a lead iodide aerosol in the supercooled cloud was inhibited to -27C at nearly this concentration. No attempt was made to substantiate Birstein's results at higher concentrations.

It is possible that lead iodide is more susceptible to amine deactivation than a silver iodide aerosol for we know the ice nucleus activity threshold temperature for the later is significantly warmer. However the much greater sensitivity of our ice crystal detection technique, supercooled sugar solution in contrast to visual detection of crystal scintillations, and the quantitative rather than qualitative evaluation of amine effect in our approach would likely cause us to find an apparently weaker degree of inhibition.

Ethylamine. Here too, our initial expectation of the extent of inhibition based on Birstein's (1957,1960) results were not met. Birstein (1960) reported an ethylamine concentration of 1 ppm sufficient to suppress ice nucleation by lead iodide aerosol to -16 C in his cloud chamber.

In contrast, our results show that at even the highest concentration used, points 2 and 3, the reduction of active silver iodide muclei is but 40 to 70%. At one part per million ethylamine has virtually no effect on ice nucleation by silver iodide. Direct comparison of lead iodide and silver iodide response to amine adsorption is perhaps, as with methylamine, not justified.

We would normally have discontinued our work with ethylamine at this point because it had ceased to be effective as a nucleation suppressant. However the incloud seeding work by Henderson and Duckering (1973) and the work by Haines (1974) on iso-propylamine at Colorado State University indicated an enhancement of ice nucleation may occur at very low amine concentration. Any release in the updraft of a cumulus

Table 5.4 Silver iodide ice nucleus inhibition results for amines in which pyrex final mixing vessels were used.

Compound	Concentration	Ice Crystal Counts: Untreated IN_u	σ_u	N_u	Treated IN_t	σ_t	N_t	t-stat t_{ut}	df	Ratio α	σ_α
1.Methylamine	3.7×10^{-4}	*433.3	115.5	3	350.	70.7	2	0.889	3	0.808	0.170
2.Ethylamine	3.7×10^{-4}	290.0	82.2	5	88.7	32.8	4				
		81.2	57.5	4	38.7	46.2	4				
		336.7	113.4	6	155.5	171.0	4				
		226.7	156.3	6	62.5	33.0	4				
		183.3	28.9	3	37.5	46.0	2				
		253.7	128.0	4	22.2	18.8	5				
		*240.0	129.8	28	68.2	83.2	23	5.484	49	0.284	0.078
3.	3.3×10^{-4}	91.6	48.5	5	61.0	29.7	2				
		52.0	31.0	7	42.8	43.7	5				
		228.0	87.6	5	111.2	95.8	4				
		*115.4	93.6	17	71.0	68.3	11	1.354	26	0.615	0.216
4.	3.7×10^{-5}	275.0	144.3	4	175.0	78.9	4				
		268.0	209.0	7	360.0	151.7	5				
		*270.5	180.2	11	277.8	146.0	9	0.097	18	1.027	0.274
5.	3.3×10^{-5}	126.0	105.0	5	82.0	37.0	3				
		55.0	8.7	3	52.3	2.5	3				
		175.0	109.0	3	200.0	0.	1				
		*120.0	94.8	11	86.1	56.6	7	0.848	16	0.718	0.247
6.	8.7×10^{-7}	41.7	30.0	3	25.5	23.2	4				
		47.7	18.0	4	46.6	21.6	5				
		82.0	10.5	4	98.0	25.9	6				
		* 58.5	25.8	11	61.5	38.9	15	0.221	24	1.051	0.221
7.	9.1×10^{-10}	50.8	28.8	5	104.4	32.6	5				
		57.0	19.8	2	64.5	26.2	2				
		* 52.6	25.0	7	93.0	34.7	7	2.500	12	1.768	0.404
8.	9.1×10^{-13}	149.2	71.9	5	167.7	52.3	4				
		134.2	53.3	5	171.2	39.8	5				
		57.0	55.4	4	114.0	121.6	2				
		*117.5	69.2	14	159.5	58.7	11	1.609	23	1.357	0.261
9.Butylamine	2.9×10^{-3}	*160.0	14.1	2	10.0	7.1	2	13.416	2	0.063	0.032
10.	1.2×10^{-3}	204.0	174.2	5	59.2	15.3	6				
		160.0	14.1	2	47.5	38.9	2				
		*191.4	143.9	7	56.3	20.3	8	2.641	13	0.294	0.092
11.	3.1×10^{-4}	*160.0	56.6	2	48.0	45.3	2	2.186	2	0.300	0.214
12.Hexylamine	2.3×10^{-4}	*290.0	124.5	5	13.2	11.6	5	4.950	8	0.046	0.020
13.	2.2×10^{-5}	*162.5	47.9	4	16.5	11.8	4	5.923	6	0.102	0.039
14.	2.3×10^{-6}	*181.2	62.5	4	118.0	48.7	5	1.713	7	0.651	0.164
15.Octylamine	1.9×10^{-5}	166.7	57.7	3	31.5	19.1	4				
		216.7	28.9	3	17.0	10.4	4				
		*191.7	49.2	6	24.3	16.2	8	9.102	12	0.127	0.033

Table 5.4 Continued

Ice Crystal Count Data

Compound	Concentration	IN_u	σ_u	N_u	IN_t	σ_t	N_t	t_{ut}	df	α	σ_α
16.	1.9×10^{-6}	118.3	17.6	3	8.3	14.6	4				
		165.0	23.8	4	151.0	123.5	8				
		115.0	59.7	4	89.2	57.8	6				
		100.0	0.	2	146.7	25.2	3				
		146.6	35.7	5	82.8	67.9	6				
		116.7	72.3	3	185.0	49.5	2				
		50.5	31.8	2	33.0	0.	1				
		172.0	74.3	5	190.0	65.6	3				
		71.4	31.8	5	90.0	42.4	2				
		3.5	2.1	2	4.7	6.4	3				
		*116.7	61.8	35	110.8	90.5	38	0.322	71	0.949	0.152
17.Dodecylamine	1.9×10^{-7}	293.8	42.7	4	230.0	77.9	5				
		202.6	81.9	7	206.7	75.1	3				
		293.8	220.2	4	317.5	211.1	4				
		*251.2	126.0	15	253.3	133.1	12	0.043	25	0.992	0.210
18.Dimethylamine	3.7×10^{-4}	*525.0	28.9	4	310.0	89.4	5	4.565	7	0.590	0.078
19a.Morpholine	7.8×10^{-4}	10.0	5.7	2	22.0	29.7	2				
		35.0	44.3	4	3.5	2.1	2				
		69.7	18.2	6	34.5	30.2	6				
		82.4	51.2	7	66.0	24.2	5				
		110.7	44.7	3	42.0	0.	1				
		* 67.6	46.4	22	39.4	31.2	16	2.105	36	0.583	0.143

*Values obtained by combining all data at that concentration.

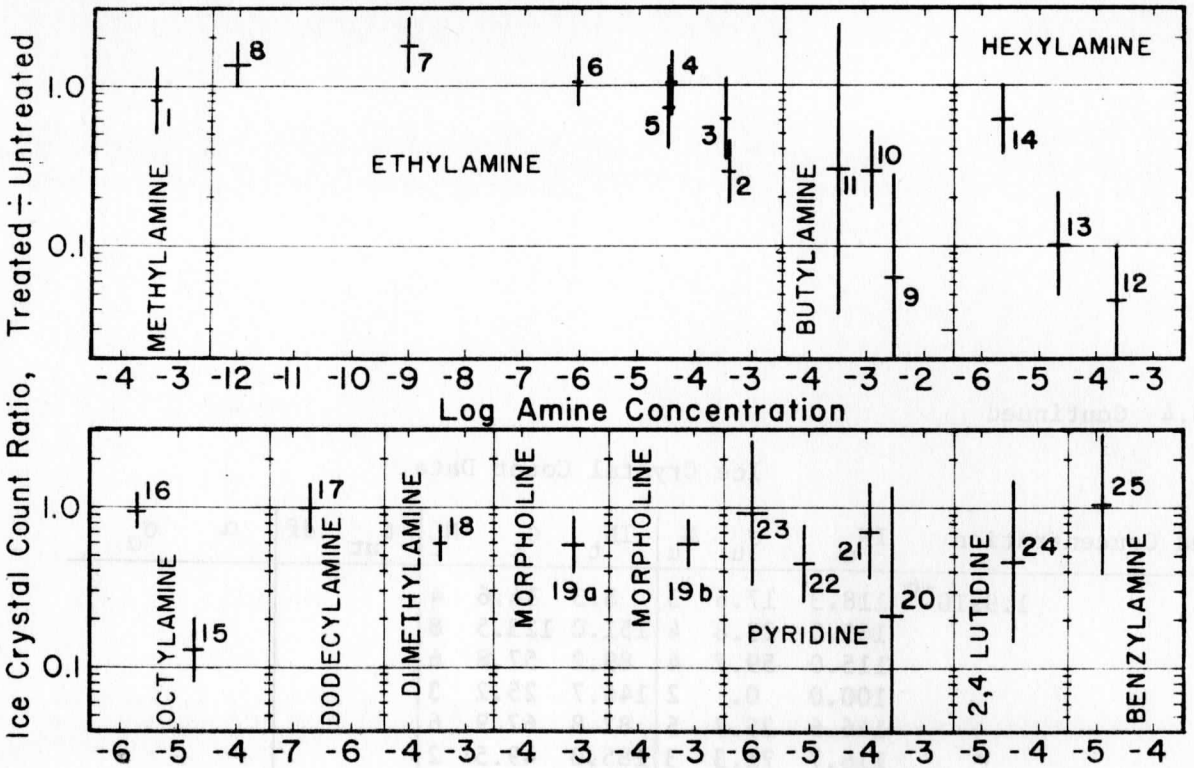

Figure 5.1. Graphical presentation of ice nucleus inhibition data for all the amines tested. Numbers refer to data in Tables 5.2, 5.4, and 5.5. Bars give 90% confidence intervals.

cloud would result in a concentration of ethylamine much less than 1 ppm. Based on the data given by Henderson and Duckering, we estimate a concentration of only 1 part in 10^{10} would exist within the treated volume; locally higher concentrations would occur near the track of amine release.

Our work indicates that at concentrations between 10^{-12} and 10^{-6} ethylamine appears to increase the number of active silver iodide ice nuclei. A maximum increase of 77% was found for point 7 at 10^{-9} concentration. At still lower concentration the enhancement also vanishes. It is interesting that Henderson and Duckering infer from their qualitative observations of the treated clouds that seeding with ethylamine stimulated rather than inhibited glaciation. Such an occurrance is possible if natural ice nuclei respond to low ethylamine concentrations in the same way as silver iodide nuclei.

Butylamine. Birstein (1957) stated that effective inhibiting substances should have a high vapor pressure to prevent condensation of the amine vapor at cloud temperatures. Yet, in any atmospheric application the concentration of amine would be far below "saturation" even at the lowest of cloud temperatures. The effectiveness of an amine as an ice nucleatant suppressant may well depend on the surface area of the potential ice nucleus occupied by an adsorbed amine molecule. This area should increase as the length of the carbon chain increases. As this chain length is increased, the vapor pressure decreases. We decided to also test the higher molecular weight amines; butylamine is the first of the liquid phase amines dealt with in our study.

Butylamine doubles the ethylamine carbon chain length. However, as is seen in Fig. 5.1, a significant improvement in ice nucleus deactivation did not accompany this change. Data point 9, while lower than 10 or 11 by a factor of 5 is also at an order of magnitude greater concentration. Data points 10 and 11 compare closely to 2 and 3 of ethylamine at nearly the same

concentration. The very large confidence interval on point 11 clearly reflects the minimal data set on which the mean value was based. Lower concentrations were not tested because of the similarity to ethylamine.

Hexylamine. In comparison to ethylamine, the carbon chain length is now tripled. At the highest concentration tested (12) hexylamine decreases the number of active nuclei by nearly a factor of ten compared to ethylamine (3) or butylamine (11). This improved performance, however, rapidly decays as the concentration decreases even though hexylamine remains the most effective substance at all concentrations tested.

The large change in deactivation between point 14 and 13 alludes to a threshold concentration at which deactivation rapidly increases. Similar features can be seen for butylamine and ethylamine. For ethylamine this break seems to come between points 4 and 3, while for butylamine it is between 10 and 9. Unfortunately the density of data points is not adequately large to show if this feature is real.

Octylamine. Extending the carbon chain length to eight leads to little increased effectiveness as an ice nucleant inhibitor. Compared to hexylamine, octylamine is even slightly less effective, especially at the lowest concentration used. The great difference between points 16 and 15 again points to the possibility that a threshold concentration exists at which octylamine begins to be effective. The very low vapor pressure of octylamine at OC kept us from trying higher concentrations.

Dodecylamine. This is the last of the primary amines tested. With 12 carbon atoms it has the longest carbon chain of the molecules tested and has the lowest OC vapor pressure. Concentrations in excess of 10^{-5} were not possible with the bubbler system at OC. At 2.8×10^{-6} concentration, we found dodecylamine to have no effect on ice nucleation.

The behavior of the various primary amines is summarized in Fig. 5.2. The value of α is given here as a function of the molecular weight of the amine. Nearly all of the amines were examined at similar concentrations so intercomparisons can easily be made of the effectiveness of each amine as an inhibitor at a given concentration. The feature which stands out here, is the pronounced minimum in α for hexylamine. A downward trend from methylamine through hexylamine is readily apparent at 4×10^{-4} concentration. At 4×10^{-5} the downward trend is still there but octylamine reverses the trend. At 4×10^{-6}, only hexylamine has an α significantly (85% level) different from unity.

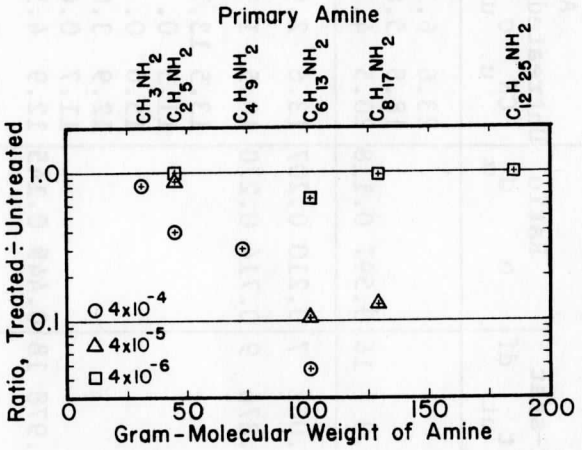

Figure 5.2. Ice crystal count ratio showing inhibition of silver iodide ice nucleation achieved by primary amines as a function of amine molecular weight; maximum deactivation by hexylamine.

5.4.2 Results for other amines

Dimethylamine. Only one simple secondary amine was examined. Although its molecular weight and density are similar to ethylamine, the differences in range of liquid phase and vapor pressures indicated dimethylamine has a reduced capacity for hydrogen bonding. Such bonding apparently plays an important role in the adsorption of amines by the aerosol. In comparison to the deactivation achieved by other substances dimethylamine was not outstanding. Birstein (1957) reported a concentration of 1.3×10^{-3} would suppress nucleation by silver iodide to -20C.

Morpholine. The substance was brought to our attention by the work of

Table 5.5 Ice nucleus inhibition results for amines in which polyethylene bag final mixing vessels were used.

Compound	Concentration	Ice Crystal Counts: Untreated IN_u	σ_u	N_u	Treated IN_t	σ_t	N_t	t-stat t_{ut}	df	Ratio α	σ_α	Aerosol Concentration: Untreated CN_u	σ_u	Treated CN_t	N_t	t-stat t_{ut}	df	Ratio β	σ_β
19b.Morpholine	7.8×10^{-4}	106.8	24.5	5	97.4	35.4	5					23.6	6.1	13.9	2.9				
		194.5	83.2	4	74.0	14.9	4					18.8	5.8	9.7	1.9				
		*145.8	70.9	9	87.0	29.4	9	2.3	16	0.597	0.118	20.5	4.7	12.0	3.2	2.000	16	0.586	0.088
20.Pyridine	2.7×10^{-4}	*147.8	213.0	5	31.0	46.4	4	1.062	7	0.210	0.207	13.6	2.9	8.8	1.8	2.874	7	0.647	0.090
21.	1.1×10^{-4}	* 29.4	19.6	5	21.0	11.9	6	0.876	9	0.714	0.270	10.5	1.3	11.4	3.5	0.573	9	1.090	0.149
22.	8.1×10^{-6}	100.0	0.	2	33.0	0.	1					13.5	13.7	11.3	0.				
		33.0	0.	1	5.0	0.	1					11.3	0.	8.5	0.				
		106.5	61.5	2	6.0	0.	1					15.0	0.	10.2	0.				
		41.0	8.2	5	45.0	7.1	2					12.9	3.0	11.3	0.				
		23.3	2.5	3	20.0	0.	2					11.7	0.6	7.4	1.6				
		* 55.5	38.6	13	24.9	17.0	7	1.978	18	0.449	0.145	12.9	4.5	9.6	1.9	1.833	18	0.744	0.091
23.	9.9×10^{-7}	5.7	8.1	3	26.0	19.8	2					10.9	0.6	8.8	3.5				
		300.0	86.6	3	216.0	28.9	3					19.8	4.8	10.4	2.0				
		*152.8	170.3	6	140.4	106.9	5	0.141	9	0.919	0.522	16.2	6.5	9.7	2.4	2.105	9	0.600	0.118
24.2,4Lutidine	3.5×10^{-5}	25.0	35.4	2	3.5	5.0	2					12.6	3.4	11.1	3.7				
		22.5	5.0	2	18.5	2.1	2					8.6	2.3	7.5	2.6				
		* 23.8	20.7	4	11.0	9.2	4	1.130	6	0.463	0.279	10.6	3.3	9.3	3.3	0.542	6	0.879	0.207
25.Benzylamine	1.3×10^{-5}	10.0	14.1	2	20.0	0.	1					18.0	0.	19.5	0.				
		100.6	91.2	5	92.8	60.5	4					16.7	4.0	16.0	4.1				
		* 74.7	86.8	7	78.2	61.6	5	0.077	10	1.047	0.589	17.1	3.4	16.7	3.9	0.180	10	0.977	0.126
35.Blank Runs	-	6.5	5.3	4	5.0	4.2	2					2.3	0.9	2.5	0.2				
		1.0	1.7	3	4.5	6.4	2					4.5	2.8	4.4	1.9				
		40.6	56.3	5	48.3	45.4	3					27.1	9.8	15.6	3.6				
		120.0	71.2	4	137.5	43.5	4					15.4	8.1	14.6	3.6				
		186.4	174.5	5	500.0	0.	2					21.4	9.3	26.0	9.1				
		316.7	28.9	3	400.0	100.0	3					35.3	5.5	31.6	3.8				
		110.0	14.1	2	100.0	0.	2					24.8	7.4	22.3	1.3				
		*108.2	128.3	26	173.0	183.7	18	1.379	42	1.599	0.546	18.5	12.8	17.2	10.3	0.358	42	0.930	0.182

*Values obtained by combining all data at that concentration.
Aerosol concentration value given in table must be multiplied by 1000 to give particles cm^{-3}.

Henderson and Duckering (1973). Morpholine has a molecular structure unlike the previous amines tested. It behaves as a secondary amine but is unusual in that the ethyl radicals are linked together by oxygen into a six-membered ring with the nitrogen and oxygen in opposition (Jefferson Chemical Company, 1968).

We began our testing of morpholine just before changing from dual glass to dual polyethylene bag final mixing vessels. Data point 19a in Fig. 5.1 is for the data obtained with the dual glass system while point 19b is with the dual bag system. The equivalence of these two points indicates the dual bag system gives reliable results. However, the 40% reduction in active ice nuclei at this high a concentration does not explain Henderson and Duckerings observations of its effect on cumulus cloud glaciation. Perhaps natural nuclei are more susceptible to deactivation by morpholine than to ethylamine at very low amine concentrations.

Pyridine. Pyridine is another heterocyclic amine; one nitrogen is substituted for one CH group in the aromatic benzene ring. At similar concentrations pyridine was found to be twice as effective as an ice nucleus inhibitor as morpholine and retained its effectiveness at even lower concentrations. However its inhibiting activity also vanished at approximately 1 ppm.

2,4 Lutidine. This compound is closely related to pyridine; 2,4 dimethyl pyridine. Metyl groups replace hydrogen at the 2 and 4 position on the six-membered ring; nitrogen occupies position 1. Several other isomers with similar properties exist. With the additional methyl groups, we had hoped 2,4 lutidine would be superior to pyridine, however, the results indicate a very similar degree of inhibition. For this reason additional concentrations were not tested.

Benzylamine. This is the only aromatic amine to be tested. Of the simple aromatic amines benzylamine has the lowest boiling point and highest basicity. Yet at the highest concentration tested no inhibition was noted.

The above four amines were tested with the dual polyethylene mixing vessels and the data on ice nuclei and aerosol concentrations were also examined by the methods of section 5.3.2. The results of this analysis are given in Table 5.6. Each amine is identified by the number in column C. Total aerosol concentration is given by CN x 10^3 particles cm^{-3} and is the geometric mean of treated and untreated aerosol for that concentration. The parameters A and B are given with their calculated standard deviations. Although the ratio $\tilde{\alpha}$ determined by this regression technique compares well in most cases with the ratio α in Table 5.5, the large standard deviation of the ratio $\tilde{\alpha}$ makes any such comparison insignificant. The large standard deviations of A and B in the regression equations are clearly the cause for the uncertainty associated with $\tilde{\alpha}$.

Total aerosol count was also measured along with ice crystal count when the dual polyethylene bag mixing vessels were used. Data analysis for the aerosol counts was similar to 5.3.1. Figure 5.3 shows the ratio of aerosol concentration in the treated and untreated bag as a function of amine concentration. In general one could conclude that some suppression of condensation nuclei also accompanies the inhibition of ice nuclei through the increased hydrophobicity of the treated aerosol.

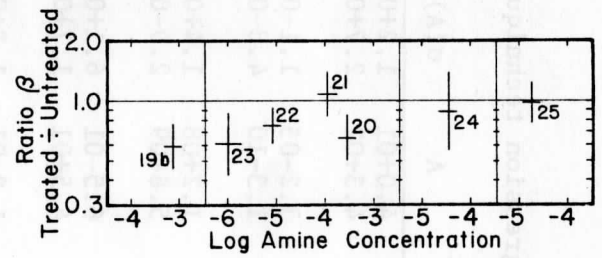

Figure 5.3. Aerosol concentration ratios for treated and untreated samples for the amines used with the polyethylene final mixing vessels. Numbers refer to data in Table 5.5.

In order to determine if passage through the bags significantly affected the aerosol count or led to different aerosol counts, we also made several days of tests with no amine entering the "treated" bag. Ice crystal counts and aerosol counts were taken just as

Table 5.6 Results of regression technique to compute ice crystal count ratios of treated and untreated samples.

C	CN	σ(CN)	T/U	A	σ(A)	B	σ(B)	R	N	IN*	σ(IN*)	t	$\tilde{\alpha}$	σ($\tilde{\alpha}$)
19b	15.3	0.9	T	4.0+01	1.2+02	0.293	1.220	0.247	9	88.9	398.4	0.045	0.602	5.717
			U	4.3+02	2.7+03	-0.392	2.066	-0.197	9	147.8	1238.2			
20	10.9	0.7	T	3.2-05	1.1-03	5.630	15.315	0.390	4	20.6	1016.2	0.018	8.621	611.949
			U	1.3-10	4.8-09	9.948	14.518	0.609	5	2.4	122.4			
21	10.7	0.7	T	1.2+08	1.4+09	-6.781	4.981	-0.830	6	12.2	206.0	0.002	0.861	62.542
			U	5.8-09	2.9-07	9.103	21.124	0.433	5	14.1	988.1			
22	10.7	0.8	T	6.5-01	6.1+00	1.447	4.159	0.363	7	22.5	305.9	0.060	0.491	7.145
			U	4.5+01	1.7+02	0.009	1.509	0.006	13	45.9	239.5			
23	12.0	1.2	T	1.2-01	1.2+00	2.933	4.454	0.593	5	175.9	2632.9	0.065	43.428	1077.592
			U	1.3-07	1.9-06	6.942	5.340	0.818	6	4.0	80.1			
24	9.5	1.1	T	1.4+06	1.3+07	-5.844	4.271	-0.845	4	2.7	35.4	0.036	0.233	5.777
			U	1.1+08	1.6+09	-7.135	6.414	-0.789	4	11.6	241.8			
25	13.4	3.6	T	5.4+00	1.1+01	0.852	0.806	0.241	5	49.3	145.9	0.035	2.993	168.470
			U	4.5-01	1.9+01	1.387	14.616	0.102	7	16.5	925.7			
35	12.6	1.9	T	3.0-01	1.3+00	2.014	1.626	0.779	18	49.2	296.9	0.083	2.346	23.235
			U	7.7-01	4.4+00	1.305	2.117	0.533	26	21.0	164.6			

C = Identifier refering to data in Table 5.5
CN,σ(CN) = Geometric mean aerosol concentration and standard deviation x 10^{-3}.
T/U = Identifies data from treated and untreated samples.
A,σ(A) = Regression line intercept and standard deviation.
B,σ(B) = Regression line slope and standard deviation.
R = Linear correlation coefficient.
N = Number of data points used in regression analysis.
IN*,σ(IN*) = Regression derived ice crystal count and standard deviation.
t = Student's t-statistic for N-2 degrees of freedom.
$\tilde{\alpha}$,σ($\tilde{\alpha}$) = Regression derived crystal count ratio and standard deviation.

though a normal test run with an amine was being made. These are the "blank" runs given in Table 5.5 identified as number 35. Ratios for ice crystal count and aerosol concentration for the "blank" runs and for the amine runs shown in Fig. 5.3 are plotted in Fig. 5.4. In either case it is apparent that there is little correlation between α and β. It is possible to account for the apparent difference between the ice nucleus populations of the two bags by dividing each ratio α by $\bar{\alpha}$ blank = 1.599. However, with a non-significant difference between the aerosol population of the two bags seen through $\bar{\beta}$ = 0.930 in Table 5.5., it was felt such a correction is not justified. If applied it would, of course, improve our evaluation of the performance of the later four amines.

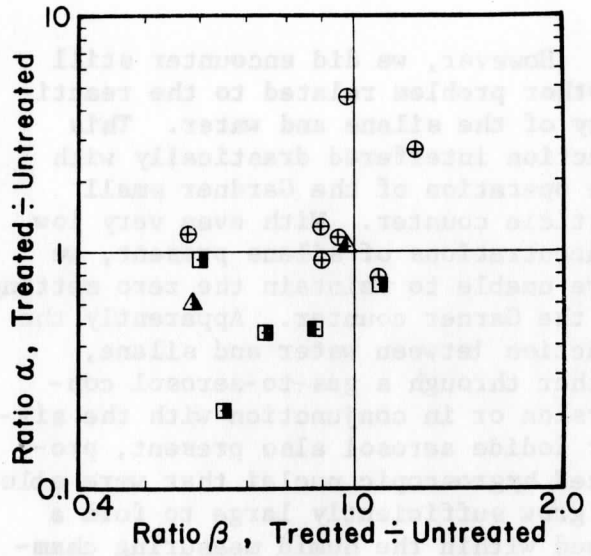

Figure 5.4. Scatter diagram showing correlation between ice crystal count ratio α and aerosol concentration ratio β. Symbols refer to legend of Fig. 5.5 while crossed circles are for blank runs.

5.5 Summary of amine results

To summarize the behavior of amines as inhibitors of ice nucleation a presentation of the degree of inhibition verses the relative pressure of amine is given in Fig. 5.5. Relative pressure is based on the concentration and saturation vapor pressure at 20C. Those amines which are effective begin to show their effectiveness at relative pressures exceeding 10^{-4}.

Seven pertinant findings relating amines to ice nuclei inhibition are:

a. Primary amines of molecular weight less than 130 do inhibit ice nucleation by silver iodide at -16C if at concentrations exceeding one part in one hundred thousand.

b. Hexylamine appears to be the most effective inhibitor of ice nucleation among the primary amines.

c. Inhibition by primary amines becomes significant after an apparent threshold concentration between 10^{-6} and 10^{-5} (relative pressure $>10^{-4}$) is attained.

d. High molecular weight (>130) amines are ineffective inhibitors.

e. Aromatic and heterocyclic amines are not efficient inhibitors of ice nucleation at the concentrations tested.

f. At very low concentrations (10^{-9}) ethylamine shows a weak enhancement of ice nucleation by silver iodide at -16C.

g. Adsorption of amines impairs the behavior of silver iodide aerosols as condensation nuclei in a Gardner small particle counter.

VI. Silanes as Ice Nucleus Inhibitors

Silanes have often been used to make surfaces hydrophobic. We decided to examine the behavior of two silanes as ice nucleus inhibitors. Properties of the silanes selected are given in Table 6.1. Dichlorodimethylsilane was used by Van Valin and Allee (1971) to stabilize laboratory clouds. They reported that several silanes stabilize clouds by depressing the saturation vapor pressure. The extent of vapor pressure depression was adequate to inhibit the nucleation and growth of ice crystals. Unchlorinated silanes showed little effect; trichlorosilanes were most effective.

6.1 Behavior of silanes in system

Both silanes were introduced via the bubblers. No problems with the bubblers were encountered. Shortly after starting to use dichlorodimethylsilane, we noticed that the mixing vessels associated with the Wösthoff

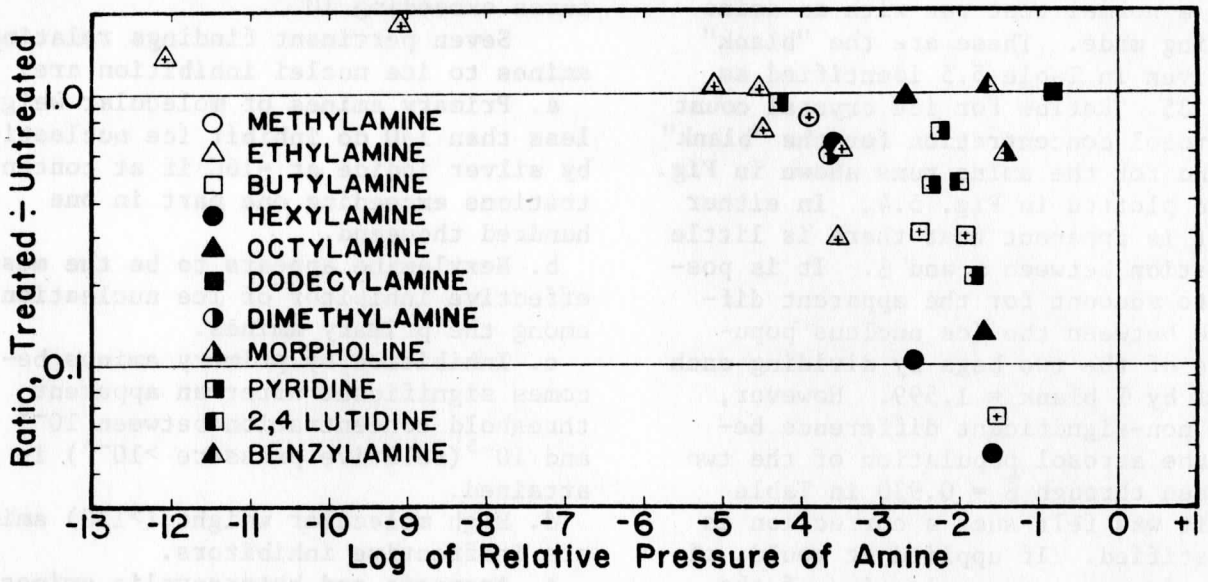

Figure 5.5. Dependence of AgI ice nucleation inhibition on the relative pressure of the amine in the final mixing vessel.

gas dosing device and the dynamic dilution vessels became coated with a translucent film. At this time, we were still using the cleansed house air supply as the carrier gas. All chlorosilanes react readily with water, even in the vapor, to form a silicone oil and hydrochloric acid. The translucent film was a coating of silicone oil deposited as the dichlorodimethylsilane reacted with water vapor in the carrier stream. As a result, we converted to dry nitrogen as the carrier gas to the dynamic dilution vessels and Wösthoff gas dosing device. No further difficulty with either silane in the dilution system was noted after this change. Our estimate of silane concentration in the final mixing vessel is given in Table 6.2.

However, we did encounter still another problem related to the reactivity of the silane and water. This reaction interfered drastically with the operation of the Gardner small particle counter. With even very low concentrations of silane present, we were unable to maintain the zero setting on the Garner counter. Apparently the reaction between water and silane, either through a gas-to-aerosol conversion or in conjunction with the silver iodide aerosol also present, produced hygroscopic nuclei that were able to grow sufficiently large to form a cloud within the humid measuring chamber with an appreciable extinction coefficient. For this reason, the aerosol concentration values reported in the following section must be regarded

Table 6.1 Properties of silanes

Compound	Formula	Molecular weight	Density gm cm^{-3}	Freezing point, C	Boiling point C	0C Vapor pressure, mb	20 C Vapor pressure, mb
Dichlorodimethylsilane	$Cl_2Si(CH_3)_2$	129.06	1.064	-86.0	70.3	54.30	146.00
Diethoxydimethylsilane	$(C_2H_5O)_2Si(CH_3)_2$	148.26	0.839	-87.0	113.5	5.63	19.81

Table 6.2 Concentration data for silanes.

Material	C	S90	PI	P	SF	FW	R(1)	R(4)
26. Dichlorodimethylsilane	8.8-04	3.5-04	5.4+01	987	0	0	60.	0.026
27. Dichlorodimethylsilane	2.5-05	1.1-05	5.4+01	979	10.	100	19.	0.020
28. Dichlorodimethylsilane	2.6-06	1.1-06	5.4+01	971	1	100	19.	0.020
29. Diethoxydimethylsilane	4.4-06	1.8-06	5.6-01	975	0	0	130.	0.021
30. Diethoxydimethylsilane	2.6-07	1.1-07	5.6-01	975	10	100	19.	0.020
31. Diethoxydimethylsilane	2.6-08	1.1-08	5.6-01	975	1	100	19.	0.020

with suspicion. These counts were made by rapidly re-zeroing the meter just prior to expansion. At the highest dichlorodimethylsilane concentration even this attempt to secure a reading failed.

6.2 Results with silanes

In contrast to the whole cloud exposure to the silane that occurred in Van Valin and Allee's experiment, only the treated nuclei and a very minute quantity of silane vapor were present in our cloud. Therefore, ice crystal nucleation suppression through vapor pressure depression can not be used as an explanation for any observed inhibition in our experiment. Unfortunately, the data obtained with the two silanes is not of high quality; too few data points and large scatter in those obtained. Table 6.3 presents a synopsis of the results. Aerosol concentration values must be multiplied by one thousand to give particles cm^{-3}; interpretation of these numbers is made very difficult by the interference of the silanes with the operation of the Gardner counter.

The limited ice crystal count data allows the following qualitative interpretation. At high dichlorodimethylsilane concentrations an apparent enhancement of ice nuclei number occurs. This enhancement changes to a noticeable inhibition at lower concentrations. Diethoxydimethylsilane behaves in a similar fashion although with a less pronounced low concentration inhibition. Unfortunately, the statistical significance of the data is so poor that these statements are statistically pure conjecture.

Our results do not conflict with the interpretation given by Van Valin and Allee (1971) of their results. Their statement that at a concentration of 2×10^{-3} dichlorodimethylsilane (i.e. 10 μℓ silane in $0.15 m^3$ of cloud) inhibited ice nucleation to -20C is based on the depression of the saturation vapor pressure by the silane. Whereas we find small concentrations of silane inhibit the ice nucleating activity of silver iodide aerosols; the distinction is noteworthy.

At low concentrations we would expect, from the active patch model of the silver iodide surface, that such patches would most actively adsorb the silane rendering the patch inactive. We lack a convincing explanation for the apparent enhancement observed at high silane concentrations. Perhaps the adsorbed silane permits more silver iodide particles to participate in condensation processes when injected into our supercooled cloud allowing more particles to act via a freezing mechanism. Even though these statements are based on scanty and noisy data it is evident that silanes deserve additional study as nucleation inhibitors.

VII. Conclusions

The elements for the quantitative examination of ice nucleus inhibition have been successfully developed and utilized. Test substance concentrations ranging from more than one part in one thousand to less than one part in 10^{12} can be easily produced in a multi-stage dynamic dilution system. Vaporous and liquid phase test substances can serve as input to the system.

An ice nucleus generator capable of long term output stability was developed by plating a nichrome filament with silver which was then conver-

Table 6.3 Silver iodide ice nucleus inhibition results for Silanes.

Compound	Concentration	Ice Crystal Count						t-stat		Ratio		Aerosol Concentration			t-stat		Ratio	
		Untreated			Treated							Untreated		Treated				
		IN_u	σ_u	N_u	IN_t	σ_t	N_t	t_{ut}	df	α	σ_α	CN_u	σ_u	CN_t	t_{ut}	df	β	σ_β
26. $Cl_2Si(CH_3)_2$	$8.8x10^{-4}$	51.0	45.6	3	58.0	0.	1											
		225.0	106.1	2	300.0	0.	1											
		*120.6	113.7	5	179.0	171.1	2	0.548	5	1.484	1.182	No data		No data				
27.	$2.5x10^{-5}$	* 68.3	7.6	3	66.0	19.8	2	0.196	3	0.966	0.214	24.4	4.4	15.8	7.8	1.361	2	0.615 0.239
28.	$2.6x10^{-6}$	*116.3	125.3	4	43.5	44.5	2	0.758	4	0.374	0.337	16.3	7.1	11.3	1.5	0.969	2	0.693 0.223
29. $(C_2H_5O)_2Si(CH_3)_2$	$4.4x10^{-6}$	*216.0	32.1	5	225.0	28.9	4	0.436	7	1.042	0.096	24.4	1.0	13.7	1.3	11.135	4	0.561 0.034
30.	$2.6x10^{-7}$	* 93.2	90.2	6	206.0	257.9	3	1.013	7	2.210	1.821	21.1	2.6	14.4	0.9	3.393	6	0.682 0.046
31.	$2.6x10^{-8}$	*161.8	86.7	4	143.0	82.0	3	0.289	5	0.884	0.376	27.5	3.4	16.4	1.5	5.152	5	0.596 0.048

ted to silver iodide through reaction with with iodine vapor. With this silver iodide aerosol as a reference standard, comparative ice nucleus counts could be made on aerosols exposed to the inhibiting agent and untreated aerosols. A quantitative index of the inhibition produced at a constant temperature and concentration could then be computed.

An isothermal, cloud settling chamber was designed to provide a water saturated environment for ice nucleation. Diffusion of water vapor through a temperature gradient in the upper one third of the chamber gave rise to the supersaturation needed to produce droplets which fell through the isothermal lower two thirds of the chamber. Ice crystals nucleated within the cloud fell into a tray of sugar solution wherein growth to visible size quickly took place.

Nearly all the substances tested were compatible with the design of this test system. However, a few materials gave rise to minor problems with the dilution system or the mixing vessel in which aerosol and test substance were combined.

The eleven amines demonstrated the ability to suppress the ice nucleation activity of our silver iodide aerosol at concentrations near one part per thousand. However, as the concentration was reduced, only hexylamine and octylamine retained activity as inhibitors to one part per million. At still lower concentrations, ethylamine affected a slight enhancement of nucleation activity at less than one part per billion; behavior of the other amines at such low concentrations was not explored.

Silanes had an impact on ice nucleation which was less clear cut than the amines and which was inverted with respect to concentration. At low concentrations an apparent inhibition of ice nucleation resulted while at higher concentrations an enhancement appeared. These observations on the silanes are based, unfortunately, on statistically meager samples. The results for the amines are much more convincing.

This study has expanded the horizons of precipitation management by identifying within the amine family the most active inhibitors of silver iodide

ice nucleation: hexylamine and octylamine. However, much work remains to be done to extend these results to natural ice nuclei. We need to identify which ice nucleation mechanism--freezing, contact, deposition--is being inhibited. More importantly, the process by which adsorbed substances interfere with ice nucleation requires considerable attention. Only with this information can we efficiently apply the concept of ice nucleation inhibition to precipitation process modification.

Acknowledgments

The support and encouragement of Dr. C. E. Anderson during all phases of this research is gratefully acknowledged. Much of the experiment was performed with the able and industrious assistance of Mr. R. S. McKenzie, my laboratory technician, and Ms. S. Curkeet, his technical aid; their efforts are deeply appreciated.

References

Axelrod, H. D., J. B. Pate, W. R. Barchet, and J. P. Lodge, Jr., 1970: Dynamic trace gas dilution system. *Atmospheric Environment*, 4, 209-212.

Birstein, S. J., 1957: Studies of effects of certain chemicals on the inhibition of nucleation. In *Artificial Simulation of Rain*, H. Weickmann and W. Smith, ed's, Pergamon Press, 376-384.

_____, 1960: Studies on the effects of chemisorbed impurities on heterogeneous nucleation. In *Physics of Precipitation*, H. Weickmann, ed., American Geophysical Union Monograph No. 5, 247-251.

Corrin, M. L., J. A. Nelson, B. Cooley, and B. Rosenthal, 1967: The preparation of "pure" silver iodide for nucleation studies. *J. A. S.*, 24, 594-595.

Feeley, E. M. and E. J. Kunnas, 1961: Heatless reactivation of desiccant dryers. *Instruments and Control Systems*, 34, 1855-1857.

Georgii, H. W., 1963: Investigations on the deactivation of inorganic and organic freezing nuclei. *Z. angen. Math. Phys.*, 14, 503-510.

Haines, R. S., 1974: *Poisoning of silver iodide ice nucleants*. Masters thesis, Colorado State University, May, 57 pp.

Henderson, T. J. and D. W. Duckering, 1973: *An applications program of chemical dispersal in small cumulus clouds*. Report to Earth and Planetary Sciences Division, Naval Weapons Center, China Lake, California, Contract N00123-72C-1723, 35 pp.

Hong, W. H. and K. A. Connors, 1968: Spectographic determination of aliphatic amines by acylation with cinnamic anhydride. *Analytical Chemistry*, 40, 1273-1276.

Jefferson Chemical Company, 1968: *Morpholine*, technical brochure. 32 pp.

Juisto, J. E., 1971: Crystal development and glaciation of a supercooled cloud. *J. Rech. Atmos.*, V(2), 69-85.

Lamb, H., 1932: *Hydrodynamics*, 6th ed., Dover Publishing Company, 585.

O'Connor, T. C. and A. F. Roddy, 1966: The production of condensation nuclei by heated wires. *J. Rech. Atmos.*, 2/3, 239-244.

Oettel, H., 1963: Toxikolgie Pyridin und derivate. *Ullman*, 14, 484.

Ohtake, T., 1971: Cloud settling chamber for ice nuclei count. In *Proceedings of the Second International Workshop on Condensation and Ice Nuclei*, August 1970, Fort Collins, Colorado, 58-60.

Poppoff, I. G. and G. W. Sharp, 1959: Inhibition of freezing nuclei by adsorbed contaminants. *J. of Meteor.*, 16, 288-294.

Reynolds, S. E., W. Hume, II, and M. McWhriter, 1952: Effects of sunlight and ammonia on action of silver iodide particles as sublimation nuclei, *B.A.M.S.*, 33, 26-31.

Sax, N. I., 1968: *Dangerous Properties of Industrial Materials*, 3rd ed. Van Nostrand Reinhold, N.Y.

Schaefer, V. J., 1949: The formation of ice crystals in the laboratory and the atmosphere. *Chem. Rev.*, 44, 291.

Twomey, S., 1958: Quantitative aspects of seeding rates for use in supercooled clouds. *Bull. Obs. Puy de Dome*, No. 2, 33.

Van Valin, C. C. and P. A. Allee, 1971: Cloud stabilization with chlorinated silanes. *J.A.S.*, 28, 1076-1078.

Vonnegut, B., 1948: Influence of butyl alcohol on shape of snow crystals formed in the laboratory. *Science*, 107, 621.

Appendix I - Vapor Pressure Data for Selected Amines and Silanes

Computation of the concentration of test substance in the output of the dilution system is, for many materials, very dependent on their saturation vapor pressure. Table AI.1 presents data on the variation of saturation vapor pressure with temperature for some of these substances.

Interpolation of the data to 0C and 20C was done for many of the substances by fitting the data to an integrated form of the Clausius-Clapeyron equation:

$$p = A\, e^{B/T} \qquad \text{AI.1}$$

where T is the Kelvin temperature and A and B are the regression parameters. Least squares curve fitting methods gave the best estimates for A and B. The data in Table AI. 1 to which this simple interpolation equation was applied are underlined. Inherent in the assumptions underlying this form of the Clausius-Clapeyron equation is the temperature invariance of the parameter B, i.e., the latent heat of vaporization. Therefore, to make the interpolation as appropriate as possible, data points were chosen over as narrow a span available to bracket the desired temperature. Double underlining is thus found for several compounds to show the data sets used in each interpolation. Results for the substances to which this interpolation is applicable are presented in Table AI.2.

Several of the amines have saturation vapor pressures which are so low that the temperatures of interest do not appear in Table AI. 1. For these amines an extrapolation scheme was devised based on the differential form of the Clausius-Clapeyron expression:

$$\frac{d\ell np}{d(1/T)} = -\frac{L}{R} = -B(T) \qquad \text{AI.2}$$

where B(T) represents the temperature variation of the latent heat of vaporization. To a first approximation:

$$B(T) = B_o + \beta T \qquad \text{AI.3}$$

with β the coefficient of temperature variation.

The data of Table AI.1 can provide an estimate of B(T) at various temperatures by converting eq AI.2 into finite difference form:

$$B(T) = -\frac{\Delta\ell np}{\Delta(1/T)} \qquad \text{AI.4}$$

Now a linear least squares regression of B(T) onto the mean temperature for the interval $\Delta(1/T)$ will yield the parameters B_o and β needed for the integration of eq. AI.2.

In its integrated form, eq. AI.2 becomes:

$$\ell n(p/p_o) = B_o\left(\frac{1}{T_o} - \frac{1}{T}\right) + \beta\, \ell n\left(\frac{T}{T_o}\right) \qquad \text{AI.5}$$

in which p_o and T_o are, respectively, the reference saturation vapor pressure and temperature from which the extrapolation of saturation vapor pressures may begin. In Table AI.3 are presented the results of this method of extrapolating the available vapor pressure data to 0C and 20C. The extrapolation for dodecylamine is by far the most tenuous.

Saturation vapor pressure data was not found for 2,4 Lutidine. However, we located information on the parameters which give the saturation vapor pressure as a function of temperature:

$$\log_{10} p(\text{mmHg}) = A - \frac{B}{t+C} \qquad \text{AI.6}$$

where t is the Celsius temperature and

A = 7.33898
B = 1733.387
C = 230.407.

These constants yield saturation vapor pressures of $P_{0C} = 0.654$ and $P_{20C} = 2.61$ mmHg for 2,4 Lutidine.

The error analysis in section 2.8 of the trace substance concentration in the output form the bubbler train depends on the value of B in eq's AI.1 and AI.5. The quantity B/T , which appears in the expression for the fractional standard deviation of output con-

Table AI.1 Temperature (°C) dependence of saturation vapor pressure for selected amines and silanes

Substance	Saturation Vapor Pressure, mm Hg										
	1	5	10	20	30	40	100	400	700	1520	3800
Methylamine	-95.8		-73.8			-56.9	-43.7	-19.7	-6.3	10.1	36.0
Ethylamine	-82.3		-58.3			-39.8	-25.1	2.0	16.6	37.7	65.3
Butylamine	-42.8		-13.6		3.9		26.8		77.8		
Hexylamine	- 6.5		25.0		47.3		74.0	112.0	132.7		
Octylamine	25.0	50.0		77.0			114.0		179.6		
Dodecylamine	86.0		127.0			155.0	184.0	225.0	259.1		
Dimethylamine	-87.7		-64.6			-46.7	-32.6	-7.1	7.4	25.0	53.9
Morpholine	-37.0		24.86	35.6	41.73	50.4	70.5	106.2	128.9		
Pyridine	-18.9		13.2			38.0	57.8	95.6	115.4		
Benzylamine	29.0	54.8	67.7			97.3	120.0	161.3	184.5		
Dichloro dimetyl silane	-53.5		-23.8			-0.4	17.5	51.9	70.3		
Diethoxy dimethyl silane	-19.1	2.4	13.3	25.3		38.0	57.6	93.2	113.5		

Data sources: Handbook of Chemistry and Physics, 47 ed, Chemical Rubber Company. Stull, D. R., 1947: Vapor pressure of pure substances - organic compounds. Industrial and Engineering Chemistry, 39(4), 517-550.

Table AI. 2 Saturation Vapor Pressure Interpolation Constants and Results for Selected Amines and Silanes.

Substance	A_o(mm)	B_o(°K)	p_o(mm)	A_{20}(mm)	B_{20}(° K)	p_{20}(mm)
Methylamine	1.13×10^8	-3178	1004.0	8.31×10^7	-3093	2178.0
Ethylamine	1.29×10^8	-3492	361.8	3.00×10^7	-3084	831.2
Butylamine	2.53×10^8	-4425	23.38	2.53×10^8	-4425	70.65
Hexylamine	7.45×10^8	-5439	1.68	7.45×10^8	-5439	6.54
Dimethylamine	8.29×10^7	-3256	550.4	7.16×10^7	-3215	1235.0
Morpholine	1.95×10^5	-2885	5.05	1.95×10^5	-2885	10.38
Pyridine	5.84×10^8	-5133	4.03	5.84×10^8	-5133	14.53
Dichlorodimethyl silane	1.05×10^8	-4032	40.57	7.97×10^7	-3958	109.1
Diethoxydimethyl silane	6.01×10^8	-5129	4.20	3.19×10^8	-4951	14.79

Table AI.3 Saturation Vapor Pressure Extrapolation Constants and Results for Selected Amines.

Substance	B_o(°K)	β	T_o(°K)	p_o(mm)	P_{OC}(mm)	P_{20C}(mm)
Octylamine	8071	-6.240	298	1	0.143	0.690
Dodecylamine	8313	-2.004	359	1	1.43×10^{-3}	9.91×10^{-3}
Benzylamine	7633	-4.625	302	1	0.100	0.488

centration, eq. 2.8.3, is tabulated in Table AI.4 for those materials introduced to the dilution system through the bubbler train. From this table a conservative estimate for all substances of the fractional standard deviation of saturation vapor pressure is 10%.

Table AI.4 Estimate of Fractional Standard Deviation of Saturation Vapor Pressure at Bubbler Output.

Material	$\lvert B/T^2 \rvert$
Butylamine	0.0593
Hexylamine	0.0729
Octylamine	0.0853
Dodecylamine	0.1041
Morpholine	0.0387
Pyridine	0.0688
2.4 Lutidine	0.0232
Benzylamine	0.0854
Dichlorodinstlyl silane	0.0540
Diethoxydimethyl silane	0.0687
Average	0.0660

Appendix II. Dilution System Concentration Computation

A computer program was written for the UNIVAC 1108 computer of the Madison Academic Computing Center for the purpose of computing the concentration of test substance obtained in the final mixing vessel. The equations on which this program, shown in Fig. AII.1, was based are found in sections 2.6-9. Several assumptions concerning the accuracy to which we can measure various parameters were made:

(1) All flowrates based on rotometer readings are accurate to 5%.
(2) All flowrates based on manometer height differences are accurate to 5%.
(3) Amine source vapor pressure is accurate to 10%.
(4) Ambient air pressure is accurate to 5%.

These assumed accuracies are extremely conservative and give the outer limit on the probable range of the calculated concentration. Numbers in parenthesis refer to the program card sequence number.

Input data (9) includes the amine vapor pressure (PI), air pressure (P), Wösthoff cycle rate (SF) and diluent flowrate (FW), and the input (FI) and diluent (FD) flowrates to each of the dilution vessels. If the bubblers are not used then PI is set equal to or greater than P. If the Wösthoff gas dosing device is not used then SF and FW are set to zero.

Initial test substance concentration (C) is computed by (12) if in (11) PI<P or by (15) if PI ≥ P. If computation depends on (12) then the initial (13) fractional variance of the concentration (VV) is VB = 0.0125 in accordance with the above assumptions; otherwise it is zero (16). If the Wösthoff unit is used SF ≠ 0 in (17) and the concentration leaving this device is given by (18) with its fractional variance increased (19) by VW = 0.00225 in accordance with the above assumptions.

Computation of the dilution by each dilution vessel proceeds after it is determined that a dilution stage is used (21), i.e. the input flow to a given stage is not equal to zero. The fractional variance of the concentration of test substance in the output of the dilution chamber is computed (23) from equation 2.6.4 and the new output concentration by (25) which is equation 2.6.2.

The final concentration and fractional variance are used to obtain the 90% confidence limit (S90) to the concentration in (29-31). Other output parameters are previously defined.

```
      DIMENSION FI(4),FD(4),R(4),L(3)
      DATA WV,VB,VR,VW/3.3E-2,12.5E-3,5.0E-3,25.5E-4/
      READ 99,N
   99 FORMAT(I2)
      PRINT 200
  200 FORMAT(1H1,/,23X,'MATERIAL',14X,6HC      S90      PI       F    SF
     1    FW    R(1)    R(2)    R(3)    R(4),/)
      DO 98 J=1,N
      READ 100,PI,F,SF,FW,(FI(I),FD(I),I=1,4),(L(K),K=1,3)
  100 FORMAT(E7.3,F5.1,F3.0,9F5.0,3A6)
      IF(PI .GE. P) GO TO 3
      C=PI/P
      VV=VB
      GO TO 4
    3 C=1.0
      VV=0.0
    4 IF(SF)6,5,6
    5 C=C*SF*WV/FW
      VV=VV+VW
    6 DO 7 I=1,4
      IF(FI(I) .LE. 0.0) GO TO 8
      R(I)=FD(I)/FI(I)
      VV=VV*(1.0+((1.0+R(I))/(1.0+R(I)-C))**2)+VR*R(I)*R(I)/
     1((1.0+R(I)-C)**2)
      C=C/(1.0+R(I)-C)
      GO TO 7
    8 R(I)=0.0
    7 CONTINUE
      V=SQRT(VV)
      S=C*V
      S90=1.64485*S
  201 PRINT 102,J,(L(K),K=1,3),C,S90,PI,F,SF,FW,(R(I),I=1,4)
  102 FORMAT(1X,19X,I2,'.',2X,3A6,4(1XE7.2),1X,F3.0,2X,F5.0,4(1XE7.2))
   98 CONTINUE
      STOP
      END
```

Fig. AII.1 Computer program for computation of test substance concentration. Card sequence number at left.